Macromolecules

ARTICLE

pubs.acs.org/Macromolecules

Quantitative Study of Fluctuation Effects by Fast Lattice Monte Carlo Simulations. 2. Homopolymer Brushes in an Implicit, Good Solvent

Pengfei Zhang and Baohui Li

School of Physics, Nankai University, Tianjin, P. R. China 300071

Qiang Wang*

Department of Chemical and Biological Engineering, Colorado State University, Fort Collins, Colorado 80523-1370, United States

ABSTRACT: Using fast lattice Monte Carlo (FLMC) simulations both in a canonical ensemble and with Wang-Landau–transition-matrix sampling, we have studied a model system of homopolymer brushes in an implicit, good solvent. Direct comparisons of the simulation results with those from the corresponding lattice self-consistent field (LSCF) theory, both of which are based on the *same* Hamiltonian (thus without any parameter-fitting between them), unambiguously and quantitatively reveal the fluctuations and correlations in the system. We have examined in detail how the chain number density C and the interaction strength N/κ (where N is the number of segments on a chain and κ is inversely proportional to the second virial coefficient characterizing the solvent quality) affect both the brush structures and thermodynamics. For our model system, the LSCF theory is exact in both limits of $C \rightarrow \infty$ and $N/\kappa \rightarrow \infty$, where there are no fluctuations or correlations. At finite C and $N/\kappa > 0$, the segmental density profile in the direction perpendicular to the grafting substrate obtained from FLMC simulations is flatter than the LSCF prediction, and the profile differences are smaller in higher dimensions. The free-end density from FLMC simulations is also lower than the LSCF prediction well inside the brush. The LSCF theory underestimates the free energy but overestimates the entropy per chain, and underestimates the internal energy per chain at small N/κ but overestimates it at large N/κ. At large C, FLMC results approach LSCF predictions at a rate of $1/C$ in most cases.

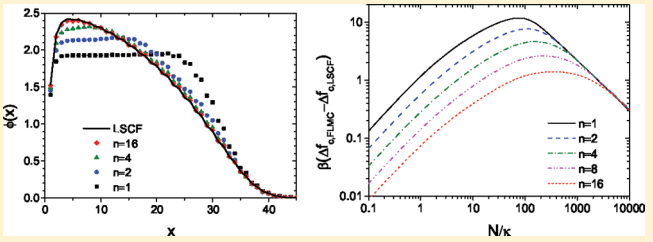

1. INTRODUCTION

Polymer brushes (polymers end-grafted on a substrate) are one of the most commonly studied polymeric systems due to their wide applications in many fields, including colloidal stabilization, surface modification, lubrication, adhesion, composite materials, stimuli-responsive surfaces, etc. There are several books,[1] many review articles,[2] and numerous research papers on polymer brushes. In this work, we limit our discussion to the simplest case of a monodisperse, uncharged and flexible homopolymer brush on a planar and nonadsorbing substrate immersed in a small-molecule solvent (either implicit or explicit); we do not consider interactions between polymers and grafting substrate, nor the cases of a compressed/stretched brush and two opposing brushes. While other theoretical formalisms, including the scaling arguments,[3,4] single-chain-mean-field theory[5] and density-functional theory,[6−8] have been applied to such systems, here we focus on the most widely used self-consistent field (SCF) theory[9] and its test by molecular simulations.

Various forms of SCF theory have been applied to the study of homopolymer brushes, which can be distinguished by their model systems, i.e., Hamiltonians including both chain model and nonbonded interactions, employed in the starting field theory and further approximations rendering the field theory tractable. As for the chain model, continuous Gaussian chains (CGC), which can be stretched infinitely, and lattice polymers, which cannot be stretched beyond their contour length, are commonly used, and chains with finite extensibility in continuum are also considered. As for the nonbonded interactions, an implicit solvent is described by the second virial coefficient v with the third virial coefficient w also needed for a poor solvent, and an explicit solvent is described by the Flory–Huggins χ parameter along with the incompressibility constraint requiring the total volume fraction of polymer and solvent to be 1 everywhere, which includes all the higher-order terms neglected in the theoretical treatment of an implicit solvent.

Dolan and Edwards first applied the continuum SCF theory (with CGC and v, referred to as CvT hereafter) to study the homopolymer brushes.[10] Whitmore and co-workers studied the case of an explicit solvent;[11−15] for their purpose of comparing with experiments, different bulk number densities for polymer segments and solvent molecules and finite-range χ interactions were used in refs 11–13. A finite-width distribution of grafting points was also used in all of their SCF calculations.[11−15] Given a model system, the only approximation in these SCF theories is

Received: June 10, 2011
Revised: July 18, 2011
Published: September 08, 2011

the mean-field approximation that ignores the fluctuations and correlations in the system.

On the basis of Semenov's classical theory[16] strictly valid in the limit of infinite stretching of CGC, Milner et al. obtained the analytical solution (referred to as IST hereafter) to CνT, where fluctuations around the most probable chain trajectory are neglected (i.e., the classical approximation).[17,18] Similar work was independently performed by Zhulina and co-workers for the cases of an explicit athermal solvent (i.e., $\chi = 0$)[19,20] and an implicit solvent described by both ν and w.[20,21] For finite stretching of CGC, Netz and Schick derived the classical theory (CT) from CνT by applying the classical approximation, which reduces to IST of Milner et al. in the limit of infinite stretching.[22,23] More recently, adapting the theory of Likhtman and Semenov for dry brushes with no solvent,[24] Kim and Matsen proposed analytical corrections to the IST of Milner et al. due to the brush depletion layer and tail region.[25] Corrections due to the finite extensibility of chains have also been incorporated in IST: Shim and Cates first modeled such chains in continuum in an explicit solvent using an ad hoc approximation;[26] Amoskov and Pryamitsyn treated freely jointed chains and chains on various lattices in an athermal explicit solvent;[27−29] and most recently Biesheuvel et al. proposed an empirical expression for freely jointed chains in an athermal solvent, where the polymer excluded-volume interactions were treated with the Carnahan−Starling equation of state.[30]

On the other hand, the lattice self-consistent field (LSCF) theory of Scheutjens and Fleer (in an explicit solvent)[31] has been applied to the homopolymer brushes by Cosgrove et al.,[32] Gorbunov and co-workers (for an athermal solvent),[33,34] Hirz,[35] Huang and Balazs (in 2D),[36] and Martin and Wang (for athermal solvents),[37] among others. Note that the Dirac δ-function interaction is used in continuum theories, except in refs 11−13 where finite-range interactions were used, and that the nearest-neighbor interaction (usually on a simple cubic lattice) is used in LSCF calculations, except in refs 38 and 39 where the Kronecker δ-function interaction was used.

The consequences of different model systems and further approximations (mainly the classical approximation) can be revealed by detailed comparisons between the various forms of SCF theory. For example, IST for chains in continuum has been compared with LSCF calculations by several groups;[17−19,26,38,39] the model differences, however, were mixed with the classical approximation and the assumption of infinite chain-stretching in these comparisons. Consequences of the classical approximation and the infinite-stretching assumption were unambiguously revealed only by Netz and Schick[23] and by Kim and Matsen,[25] who compared CνT, CT, and IST using exactly the same model system.

To reveal the consequences of the mean-field approximation inherent in all SCF theories, comparisons with molecular simulations are needed. Molecular dynamics,[40−47] Brownian dynamics,[48] dissipative particle dynamics,[49] lattice Monte Carlo (MC),[15,50−58] and off-lattice MC[44,59−61] simulations have been performed for the homopolymer brushes in a solvent. Due to its analytical results, IST for CGC in an implicit solvent[17,18,20,21] has been most commonly compared with molecular simulations.[30,40,41,43−45,50,52,53,58,62] In addition, Pépin and Whitmore compared their lattice MC simulations with continuum SCF calculations both in an explicit and good solvent,[15] Seidel and Netz compared their molecular dynamics simulations with CνT,[43] and Kreer et al. compared molecular dynamics, off-lattice MC, and lattice MC simulations with CνT.[44]

While these molecular simulations have provided important insights and greatly furthered our understanding of polymer brushes, we note that they have examined only structures (e.g., segmental distributions, brush height, and bond orientation) but not thermodynamics (e.g., internal energy, free energy, and entropy) of the brushes. To the best of our knowledge, only Ohno et al. obtained the entropy and related Helmholtz free energy of homopolymer brushes in an athermal solvent in their lattice MC simulations.[56] Furthermore, none of the above comparisons was done using exactly the same model system in both SCF theories and molecular simulations. They therefore could not unambiguously distinguish the model differences from the consequences of the mean-field approximation. There are several differences between the model systems in molecular simulations and the continuum SCF theories used in these comparisons: (1) While CGC was used in the theories, chains of finite extensibility (i.e., lattice polymers and chains in continuum with either a fixed bond length[59] or the finite extensible nonlinear elastic bonding potential) have been used in the simulations, except that the discrete Gaussian chains were used in refs 48, 60, and 61 and that chains with a harmonic bonding potential was used in ref 49. This difference in chain models is significant when chains are strongly stretched, as in a good solvent or at high grafting densities. (2) While the nonbonded interactions due to solvent were described by the Dirac δ-function interaction (which is "soft" and allows particle overlapping) in the theories, finite-range and sometimes anisotropic (as in all the lattice MC simulations and ref 61) interactions were used in the simulations with hard-core repulsions that prevent particle overlapping, except in refs 48, 60, and 61 where soft potentials[63] were used. This difference in nonbonded interactions is significant when the polymer segmental density is high, as in a poor solvent or at high grafting densities. (3) While the grafting substrate has no energetic interactions in the theories, a repulsive substrate has to be used in all the molecular dynamics, Brownian dynamics, and dissipative particle dynamics simulations. This difference is in general not significant except very close to the substrate. (4) While the SCF calculations were done in 1D under the assumption of lateral homogeneity except in ref 36 where they were done in 2D, the simulations were done in 3D with either regularly or randomly placed grafting points. This difference is significant when the lateral inhomogeneity is large, as in a poor solvent[41,46,53,55,59,61] or at low grafting densities. These model differences, although easy to understand qualitatively, are difficult to be unambiguously quantified and separated from the consequences of the mean-field approximation in the aforementioned comparisons. Last but not least, when IST is compared with molecular simulations, consequences of the classical approximation and the infinite-stretching assumption are mixed with and again difficult to be unambiguously quantified and separated from those of the mean-field approximation.

In this work, we compare fast lattice Monte Carlo (FLMC) simulations[64] and the corresponding LSCF calculations using exactly the same model system, to unambiguously quantify the system fluctuation/correlation effects ignored by the mean-field approximation on both the brush structures and thermodynamics. This is the second paper in our series of studies with such purpose. In our first paper (referred to as paper 1 hereafter), we quantified the fluctuation/correlation effects in a simple, homogeneous system of compressible homopolymer melts (or equivalently, homopolymers in an implicit, good solvent).[65] Here we study the corresponding inhomogeneous system of homopolymer brushes in an implicit, good solvent. Homopolymer brushes in an explicit solvent with varying quality are examined in a subsequent paper

in our series.[66] These studies are the prerequisite for developing more accurate theories for polymer brushes.

2. SIMULATION AND THEORETICAL FORMALISMS

2.1. Model System. We consider a homopolymer brush system of n chains each having N segments in an implicit, good solvent on a lattice, which has $L = N$ lattice layers in the x direction. The first segment of all chains is grafted at $x = 1$ (i.e., in the first layer), and an impenetrable wall is placed at $x = 0$, which cannot be occupied by polymer segments. The canonical-ensemble partition function of the system is

$$\mathscr{Z} = \frac{1}{n!}\prod_{k=1}^{n}\prod_{s=1}^{N}\sum_{\mathbf{R}_{k,s}} \cdot \exp(-\sum_{k=1}^{n}\beta h_k^{\mathrm{C}} - \beta\mathscr{H}^{E}) \tag{1}$$

where $\mathbf{R}_{k,s}$ denotes the lattice position of the sth segment on the kth chain, "$\cdot$" means that the products before it do not apply to the term after it but the summation before it does, and $\beta \equiv 1/k_{\mathrm{B}}T$ with k_{B} being the Boltzmann constant and T the absolute temperature. h_k^{C} is the Hamiltonian of the kth chain due to its chain connectivity; $\beta h_k^{\mathrm{C}} = 0$ if the chain connectivity is maintained, and ∞ otherwise. Finally, the system Hamiltonian due to nonbonded interactions is given by

$$\beta\mathscr{H}^{E} = \frac{1}{2\kappa\rho_0}\sum_{\mathbf{r}}[\hat{\rho}(\mathbf{r}) - \rho_0]^2 \tag{2}$$

where $\rho_0 \equiv nN/V$ is the average segmental density with V being the total number of lattice sites, and the microscopic density of polymer segments at lattice site $\mathbf{r}$ is $\hat{\rho}(\mathbf{r}) \equiv \sum_{k=1}^{n}\sum_{s=1}^{N}\delta_{\mathbf{r},\mathbf{R}_{k,s}}$ with $\delta_{\mathbf{r},\mathbf{R}_{k,s}}$ denoting the Kronecker δ-function. Known as the Helfand compressibility,[67] κ is equivalent to the second virial coefficient $v = 1/\kappa\rho_0$ denoting the solvent quality; $N/\kappa = 0$ corresponds to the θ-solvent, while a positive value corresponds to a good solvent. As in paper 1, N/κ here is a physical parameter while N is merely a model parameter quantifying the chain discretization.

2.2. Fast Lattice Monte Carlo Simulations. *2.2.1. Canonical-Ensemble Simulations.* Some of our FLMC simulations are performed in a canonical ensemble, where n, V, and κ are fixed. While most of our simulations are performed on a 1D lattice, we have also used various 2D and 3D lattices with L_b lattice sites in the y (and z in 3D) direction along which periodic boundary conditions are applied; we therefore have $V = L_b^{d-1}L$, where d denotes the system dimensionality. For all the simulations in 2D and 3D, one chain is grafted at every lattice site at $x = 1$ (i.e., $n = L_b^{d-1}$), which ensures the lateral homogeneity of our system and thus the direct comparisons with our 1D LSCF calculations discussed below.

Two types of biased trial moves, the simple configurational bias (SCB) and topological configurational bias (TCB) moves,[68] occurring with a probability of 0.1 and 0.9, respectively, are employed in our simulations. In SCB trial moves, we cut and regrow a partial chain of $l_{\mathrm{S}} = 5$ segments from the free end of a randomly chosen chain and accept the trial move according to the criterion of $\mathscr{P}_{\mathrm{acc}}^{\mathrm{CB}}(\mathrm{o}\rightarrow\mathrm{n}) = \min[1, R_{\mathrm{o}}/R_{\mathrm{n}}]$, where R_{n} and R_{o} are the Rosenbluth weight[68] of the trial (n) and old (o) configurations, respectively. In TCB trial moves, an inner section of $l_{\mathrm{T}} = 7$ segments of a randomly chosen chain is cut and regrown; the acceptance criterion is the same as that for SCB trial moves, except that the Rosenbluth weight now includes a bias to satisfy the chain connectivity constraint.[68] About $(2.5-20) \times 10^6$ Monte Carlo steps (MCS), which depend on n, N, and κ, are performed in each simulation, where one MCS is defined as nN trial moves. The error bar of each ensemble-averaged quantity is estimated in the same way as in paper 1.[65]

2.2.2. Wang-Landau−Transition-Matrix (WL-TM) Sampling. As in paper 1, we use the combined WL-TM sampling[69−71] to estimate the density of states (DoS) $\Omega(E)$ on the 1D lattice, defined as the number of microstates having the same $E \equiv \Sigma_{\mathbf{r}}[\hat{\rho}(\mathbf{r}) - \rho_0]^2$, within a chosen E range. Note that $\Omega(E) = 0$ for odd E in our simulations, and such macrostates are thus not included here. We use the same biased trial moves as in our canonical-ensemble simulations. At the beginning of WL-TM sampling, an array $\mathbf{g}(E)$ is set to unity, and a matrix $\mathbf{C}(E,E')$ used to estimate the transition probability from macrostate E to E' is set to zero; they are updated during the simulation. The details of our WL-TM sampling are given in paper 1.[65] Due to the biased trial moves, however, the following acceptance criteria must be used

$$\mathscr{P}_{\mathrm{acc}}^{\mathrm{WL}}(\mathrm{o}\rightarrow\mathrm{n}) = \min\left[1, \frac{\mathbf{g}(E_{\mathrm{o}})R_{\mathrm{n}}^{\infty}}{\mathbf{g}(E_{\mathrm{n}})R_{\mathrm{o}}^{\infty}}\right] \tag{3}$$

$$\mathscr{P}_{\mathrm{acc}}^{\mathrm{TM}}(\mathrm{o}\rightarrow\mathrm{n}) = \min\left[1, \frac{\hat{T}^{\infty}(E_{\mathrm{n}}\rightarrow E_{\mathrm{o}})R_{\mathrm{n}}^{\infty}}{\hat{T}^{\infty}(E_{\mathrm{o}}\rightarrow E_{\mathrm{n}})R_{\mathrm{o}}^{\infty}}\right] \tag{4}$$

where R_{n}^{∞} and R_{o}^{∞} are the Rosenbluth weights at infinite temperature (i.e., $\beta = 0$)[68,72] with $\hat{T}^{\infty}$ given in paper 1, instead of eqs 3 and 6 in paper 1, respectively. In addition, the $\mathbf{C}$-matrix is now updated according to[71]

$$\begin{aligned}\mathbf{C}(E_{\mathrm{o}},E_{\mathrm{n}}) &\rightarrow \mathbf{C}(E_{\mathrm{o}},E_{\mathrm{n}}) + \min\left[1, \frac{R_{\mathrm{n}}^{\infty}}{R_{\mathrm{o}}^{\infty}}\right] \\ \mathbf{C}(E_{\mathrm{o}},E_{\mathrm{o}}) &\rightarrow \mathbf{C}(E_{\mathrm{o}},E_{\mathrm{o}}) + 1 - \min\left[1, \frac{R_{\mathrm{n}}^{\infty}}{R_{\mathrm{o}}^{\infty}}\right]\end{aligned} \tag{5}$$

instead of eq 4 in paper 1. If the trial configuration is out of the E window specified in the simulation, it is rejected and the $\mathbf{C}$-matrix is updated according to $\mathbf{C}(E_{\mathrm{o}},E_{\mathrm{o}}) \rightarrow \mathbf{C}(E_{\mathrm{o}},E_{\mathrm{o}}) + 1$, as in paper 1.

Note that $\mathbf{g}(E)$ obtained from WL-TM simulations has a undetermined factor, so we normalize it such that $\mathbf{g}(E{=}0) = 1$. Because the density of the ground state of our n-chain brush system in 1D (where all the chains are fully stretched) is $\Omega_0(n) \equiv \Omega(E{=}0;n) = 1/n!$, we have $\Omega(E) = \mathbf{g}(E)/n!$ (for conciseness, the explicit dependence of $\Omega(E)$ and $\mathbf{g}(E)$ on n is omitted in our notation); readers are referred to paper 1 for more details.

Once $\mathbf{g}(E)$ is obtained, we can compute the Helmholtz free energy per chain

$$\begin{aligned}\beta f_{\mathrm{c,FLMC}}(N/\kappa) &\equiv -\frac{\ln \mathscr{Z}(N/\kappa)}{n} \\ &= -\frac{1}{n}\ln\sum_{E}\frac{\mathbf{g}(E)}{n!}\exp\left(-\frac{C}{2}\frac{N}{\kappa}\frac{E}{{\rho_0}^2}\right)\end{aligned} \tag{6}$$

where $C \equiv n/V$ denotes the chain number density, and any canonical-ensemble average as a function of N/κ. For the latter, we define the normalized probability distribution of E at N/κ as

$$P(E,N/\kappa) = \frac{\mathbf{g}(E)}{n!}\exp\left(-\frac{C}{2}\frac{N}{\kappa}\frac{E}{{\rho_0}^2}\right)\Big/\mathscr{Z}(N/\kappa) \tag{7}$$

The internal energy per chain is then

$$\beta u_{c,FLMC}(N/\kappa) \equiv \frac{\langle \beta \mathscr{H}^E(N/\kappa)\rangle}{n} = \frac{1}{2N}\frac{N}{\kappa}\frac{\langle E(N/\kappa)\rangle}{{\rho_0}^2} = \frac{1}{2N}\frac{N}{\kappa}\sum_E \frac{E}{{\rho_0}^2} P(E,N/\kappa) \quad (8)$$

and the entropy per chain can be obtained from the thermodynamic relation

$$s_c(N/\kappa)/k_B = \beta u_c(N/\kappa) - \beta f_c(N/\kappa) \quad (9)$$

Finally, the canonical-ensemble average of the mean-square chain end-to-end distance in the x direction ${R_{e,FLMC}}^2$ is calculated as

$${R_{e,FLMC}}^2(N/\kappa) \equiv \sum_E \overline{{R_e}^2}(E)\, P(E,N/\kappa) \quad (10)$$

where $\overline{{R_e}^2}(E) \equiv \sum_j {R_{e,j}}^2 \delta_{E_j,E}/\sum_j \delta_{E_j,E}$ is the microcanonical-ensemble average of ${R_{e,j}}^2$ over all the configurations sampled during the WL-TM simulation that belong to the macrostate E, ${R_{e,j}}^2 \equiv \sum_{k=1}^{n}(X_{k,N}-1)^2/n$ for configuration j, and $X_{k,s}$ denotes the x-coordinate of the sth segment on the kth chain. The canonical-ensemble average of brush height $h_{FLMC}(N/\kappa)$ and the mean-square chain radius of gyration in the x direction ${R_{g,FLMC}}^2(N/\kappa)$ are calculated in a similar way, with $h_j \equiv 2\sum_{x=1}^{L}(x-1)\hat{\rho}(x)/nN$ and ${R_{g,j}}^2 = \sum_{k=1}^{n}\sum_{s=1}^{N-1}\sum_{t=s+1}^{N}(X_{k,s}-X_{k,t})^2/nN^2$.

2.3. Lattice Self-Consistent Field Calculations. Because the brushes in our 2D and 3D simulations are laterally homogeneous, they can be directly compared to 1D LSCF calculations performed in the x direction. To formulate the corresponding LSCF theory with the *same* Hamiltonian as in our FLMC simulations, we insert in eq 1 the identity $1 = (\rho_0/2\pi)^L \int \mathrm{d}\phi\, \mathrm{d}\boldsymbol{\omega}\, \exp\{\mathrm{i}\boldsymbol{\omega}\cdot[\rho_0\phi - \hat{\boldsymbol{\rho}}]\}$, where $\hat{\boldsymbol{\rho}} \equiv \{\hat{\rho}(x)\}$ is a vector of L elements, $\boldsymbol{\phi} \equiv \{\phi(x)\}$ is the normalized segmental density (volume fraction) field constrained to $\hat{\boldsymbol{\rho}}/\rho_0$, and $\boldsymbol{\omega} \equiv \{\omega(x)\}$ is the conjugate field imposing the constraint. We finally have $\mathscr{Z} = (\rho_0/2\pi)^L \int \mathrm{d}\phi\, \mathrm{d}\boldsymbol{\omega}\, \exp\{-n\beta f_c[\phi,\omega]\}$ with

$$\beta f_c = \frac{1}{L}\sum_{x=1}^{L}\left\{\frac{N}{2\kappa}[\phi(x)-1]^2 - \mathrm{i}\omega(x)\,\phi(x)\right\} - \ln Q[\mathrm{i}\omega] - \frac{\ln(G^n/n!)}{n} \quad (11)$$

where we have rescaled variables according to $N\boldsymbol{\omega} \rightarrow \boldsymbol{\omega}$ and defined the single-chain partition function $Q[\mathrm{i}\omega] \equiv \prod_{s=1}^{N}\Sigma_{X_s}\cdot \exp[-\beta h^C - \mathrm{i}\sum_{s=1}^{N}\omega(X_s)/N]/G$ with $G \equiv \prod_{s=1}^{N}\Sigma_{X_s}\cdot \exp(-\beta h^C) = z^{N-1}L$ and z denoting the lattice coordination number; note that $GQ^{id} = \Sigma_E \mathbf{g}(E,n{=}1)$ (i.e., the total number of conformations of a single grafted chain) with $Q^{id} \equiv Q(N/\kappa{=}0)$.

The LSCF equations are obtained by setting $\delta\beta f_c/\delta\phi(x) = \delta\beta f_c/\delta\mathrm{i}\omega(x) = 0$ (i.e., the mean-field approximation[9]) and given by

$$\mathrm{i}\omega(x) = \frac{N}{\kappa}[\phi(x)-1] \quad (12)$$

$$\phi(x) = \sum_{s=1}^{N}\phi_s(x) \quad (13)$$

$$\phi_s(x) = \frac{\exp[\mathrm{i}\omega(x)/N]}{q_N^*(x{=}1)} q_s(x)\, q_{N+1-s}^*(x) \quad (14)$$

where $\phi_s(x)$ is the normalized density profile of the sth segment on the chain, the propagator $q_s(x)$ corresponds to the probability of finding a partial chain of s segments starting from the grafted end and ending at x in the system, and $q_t^*(x)$ corresponds to the probability of finding a partial chain of $t \equiv N+1-s$ segments starting from the free end anywhere in the system and ending at x. According to the chain connectivity, we have the recursive relations

$$q_{t+1}^*(x) = \exp[-\mathrm{i}\omega(x)/N]\{[(1-z_0)/2][q_t^*(x-1) + q_t^*(x+1)] + z_0 q_t^*(x)\} \quad (15)$$

$$q_{s+1}(x) = \exp[-\mathrm{i}\omega(x)/N]\{[(1-z_0)/2][q_s(x-1) + q_s(x+1)] + z_0 q_s(x)\} \quad (16)$$

with the initial conditions $q_1^*(x) = \exp[-\mathrm{i}\omega(x)/N]$ and $q_1(x) = \exp[-\mathrm{i}\omega(x)/N]\delta_{x,1}$ and the boundary conditions $q_s(x) = q_t^*(x) = 0$ for $x < 1$ and $x > L$, and $Q = q_N^*(x=1)/L$. Here z_0 is the fraction of the nearest-neighbor lattice sites that are at the same x of a given lattice site; for example, $z_0 = 0$ for both the 1D lattice and 3D body-centered cubic (BCC) lattice, and $z_0 = 1/3$ for both the 2D hexagonal (HEX) and 3D face-centered cubic (FCC) lattices.

We solve the LSCF equations using the Broyden method combined with a globally convergent strategy,[73] where the residual errors of eq 12 at all x are less that 10^{-12}. We then calculate the propagator $Q_{p,s}(x|x')$, which corresponds to the probability of finding a partial chain of $s+1$ segments that starts at x' and ends at x in the obtained conjugate field $\omega(x)$, from the following equation analogous to eqs 15 and 16

$$Q_{p,s+1}(x|x') = \exp[-\mathrm{i}\omega(x)/N]\{[(1-z_0)/2][Q_{p,s}(x-1|x') + Q_{p,s}(x+1|x')] + z_0 Q_{p,s}(x|x')\} \quad (17)$$

with the initial condition of $Q_{p,s=0}(x|x') = \exp[-\mathrm{i}\omega(x)/N]\delta_{x,x'}$ and appropriate boundary conditions. The mean-square chain radius of gyration in the x direction can finally be computed as

$${R_{g,LSCF}}^2 = \frac{1}{N^2}\sum_{s'=1}^{N-1}\sum_{s=s'+1}^{N}\left\{\left[\sum_{x=1}^{L}\sum_{x'=1}^{L}\exp\left[\frac{\mathrm{i}\omega(x)+\mathrm{i}\omega(x')}{N}\right] \times q_{N+1-s}(x)\, Q_{p,s-s'}(x|x')\, q_{s'}^*(x')(x-x')^2\right] \Big/ \left[q_N^*(x=1)\right]\right\} \quad (18)$$

where the term in the summation with $s' = 1$ and $s = N$ is the mean-square chain end-to-end distance in the x direction ${R_{e,LSCF}}^2$.

Once the LSCF equations are solved at a given N/κ, we calculate

$$\beta\Delta f_{c,LSCF} \equiv \beta f_{c,LSCF} - \beta f_{c,LSCF}(N/\kappa = 0) = \frac{1}{2L}\frac{N}{\kappa}\sum_{x=1}^{L}[1-\phi(x)^2] - \ln\frac{Q}{Q^{id}} \quad (19)$$

$$\frac{E_{LSCF}}{{\rho_0}^2} \equiv \sum_{x=1}^{L}[\phi(x)-1]^2 \quad (20)$$

$$\beta u_{c,LSCF} = \frac{1}{2N}\frac{N}{\kappa}\frac{E_{LSCF}}{{\rho_0}^2} \quad (21)$$

$$\frac{s_{c,LSCF}}{k_B} = \beta u_{c,LSCF} - \beta f_{c,LSCF} = \frac{1}{L}\frac{N}{\kappa}\sum_{x=1}^{L}[\phi(x)^2 - \phi(x)] + \ln Q + \frac{\ln(G^n/n!)}{n} \quad (22)$$

$$h_{LSCF} \equiv \frac{2}{L}\sum_{x=1}^{L}(x-1)\phi(x) \quad (23)$$

as well as ${R_{e,LSCF}}^2$ and ${R_{g,LSCF}}^2$.

In the limit of $N/\kappa \rightarrow \infty$, the system is in the ground state with $\phi(x) = 1$ for $1 \le x \le N$. In this case, all chains must have the same conformation, which is the most extended in the x direction (i.e., $X_{s+1} = X_s + 1$); the total number of such conformations (of a single grafted chain) is given by $GQ(N/\kappa \rightarrow \infty) = [z(1 - z_0)/2]^{N-1}$. We therefore have

$$\beta\Delta f_{c,LSCF} = \ln(GQ^{id}) - (N-1)\ln\frac{z(1-z_0)}{2} \quad (24)$$

$${E_{LSCF}}/{{\rho_0}^2} = \beta u_{c,LSCF} = 0 \quad (25)$$

$$\frac{s_{c,LSCF}}{k_B} = (N-1)\ln\frac{z(1-z_0)}{2} - \frac{\ln n!}{n} \quad (26)$$

$h_{LSCF} = N - 1$, ${R_{e,LSCF}}^2 = (N-1)^2$, and ${R_{g,LSCF}}^2 = (N^2-1)/12$ in this limit.

3. RESULTS

Our results presented here are for chains of $N = 60$ segments on a 1D lattice, except that in section 3.2.3 we present canonical-ensemble simulation results in 2D and 3D. Qualitatively the same results are also obtained for chains of $N = 20$ and thus not shown. We also note that N/κ is varied in this work by varying κ at a given N.

3.1. Density of States and Error Estimation. Figure 1 shows the density of states $\mathbf{g}(E)$ obtained from WL-TM simulations for systems with various n. We see that $\mathbf{g}(E)$ increases with increasing E at small E and decreases at large E, and that $\mathbf{g}(E)$ oscillates slightly at large E due to the use of a lattice. In addition, the range of E is broader for systems with larger n, as expected. The normalized probability distribution function $P(E,N/\kappa)$ is also shown in Figure 1 for the $n = 16$ system at $N/\kappa = 0$ and 500; we see that E of those states contributing significantly to the canonical-ensemble averages decreases with increasing N/κ (as expected, only the ground state of $E = 0$ contributes in the limit of $N/\kappa \rightarrow \infty$), and that the E ranges we choose are broad enough for computing canonical-ensemble averages in the range of N/κ from 0 to ∞. These results are consistent with the homogeneous melts studied in paper 1.[65]

As in paper 1, we define the error in $\beta f_{c,FLMC}(N/\kappa)$ as

$$\varepsilon_f(N/\kappa) \equiv \frac{1}{n}\left|\ln\sum_E \mathbf{g}(E)\exp\left(-\frac{C}{2}\frac{N}{\kappa}\frac{E}{{\rho_0}^2}\right) - \ln\sum_E \mathbf{g}_{exact}(E)\exp\left(-\frac{C}{2}\frac{N}{\kappa}\frac{E}{{\rho_0}^2}\right)\right| \quad (27)$$

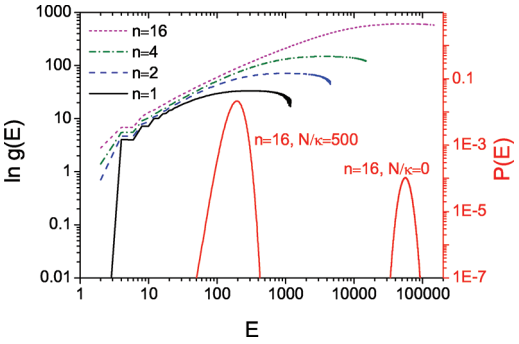

Figure 1. Density of states $\mathbf{g}(E)$ (the upper four curves) and the normalized probability distribution function $P(E,N/\kappa)$ (the lower two curves) obtained from WL-TM simulations. Note that $\mathbf{g}(E) = 0$ for odd E and we omit such points, as well as those points at large E where $\mathbf{g}(E) = 0$. In addition, $\mathbf{g}(E=2) = 1$ for the single-chain system.

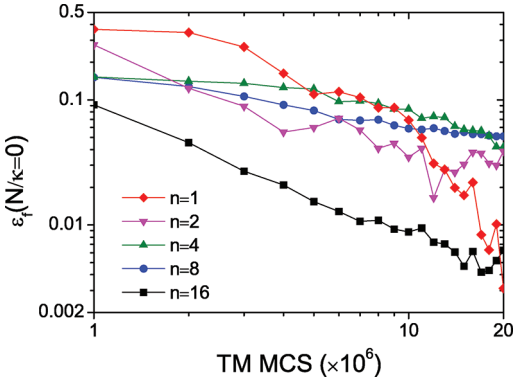

Figure 2. log−log plot of the error in the free energy per chain, $\varepsilon_f(N/\kappa=0)$, as a function of the number of Monte Carlo steps of the transition-matrix sampling, TM MCS, in our WL-TM simulations.

where $\mathbf{g}(E)$ is obtained from WL-TM simulations and $\mathbf{g}_{exact}(E)$ is the exact result. For the single-chain system of $N = 20$ on the 1D lattice, $\mathbf{g}_{exact}(E)$ can be obtained by enumeration; we then see that $\varepsilon_f(N/\kappa = 0)$ decreases with increasing number of MCS in TM simulations[65] (TM MCS) and that ε_f decreases monotonically with increasing N/κ (data not shown), as expected and also found in paper 1.[65] We can therefore use the error in $\beta f_c^{id} \equiv \beta f_c(N/\kappa=0)$ as an upper limit of ε_f.

We can also use the following formula to examine the accuracy of our WL-TM simulations:

$$\beta f_c^{id}(n) = -\frac{1}{n}\ln\sum_E \mathbf{g}(E;n) + \frac{\ln n!}{n} = -\ln(GQ^{id}) + \frac{\ln n!}{n} \quad (28)$$

where the second equal sign results from the fact that, at $N/\kappa = 0$, chains do not interact with each other and are thus uncorrelated. LSCF theory therefore gives the exact βf_c^{id}, e.g., $\beta f_c^{id} - \ln n!/n = -\ln(GQ^{id}) \approx -38.62$ for $N = 60$ on the 1D lattice. Figure 2 shows $\varepsilon_f(N/\kappa = 0) = |\ln\Sigma_E\mathbf{g}(E) - \ln(GQ^{id})|/n$ as a function of TM MCS for systems with various n. We see that, with increasing TM MCS, $\varepsilon_f(N/\kappa=0)$ decreases on average and is less than 0.06 at 2×10^7 TM MCS in all the cases. We therefore use 2×10^7 TM MCS in our WL-TM simulations hereafter.

dx.doi.org/10.1021/ma201310e |Macromolecules 2011, 44, 7837–7852

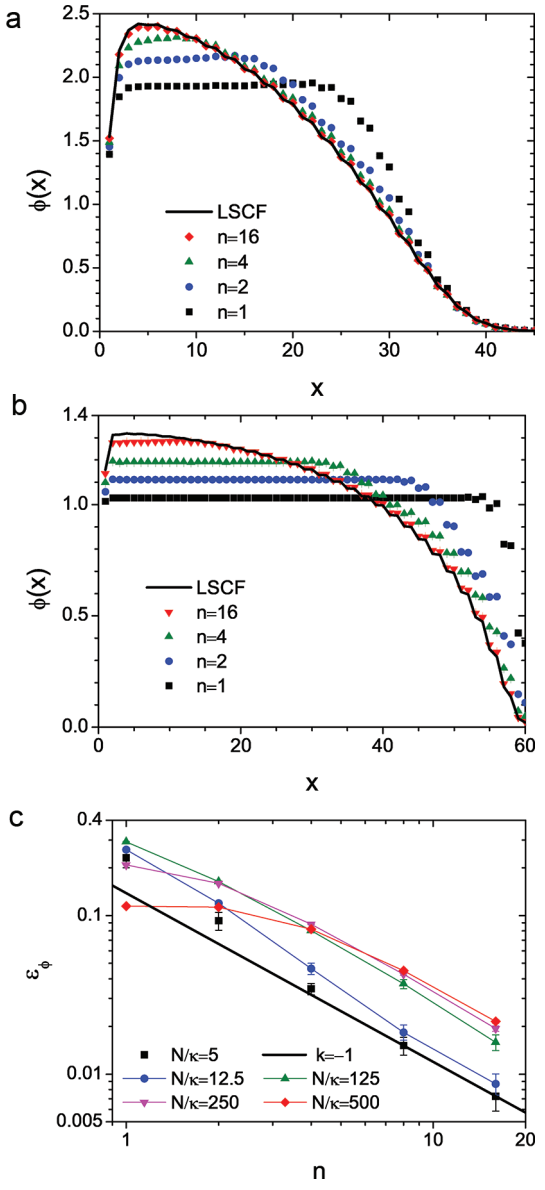

Figure 3. Polymer segmental density profiles $\phi(x)$ obtained from canonical-ensemble simulations on the 1D lattice with various n and the corresponding LSCF predictions at (a) $N/\kappa = 12.5$ and (b) $N/\kappa = 125$. (c) shows how the difference in $\phi(x)$ between FLMC and LSCF results, ε_ϕ, varies with n, where "$k = -1$" denotes a straight line of slope -1.

3.2. Brush Structures. *3.2.1. Segmental Density Profile and Brush Height.* At $N/\kappa = 0$, the ensemble-averaged segmental density profile $\phi(x)$ from our canonical-ensemble simulations coincides completely with the LSCF prediction (data not shown). In this case, polymer segments do not interact with each other and the chains are uncorrelated; because LSCF theory includes all possible chain conformations, it gives the exact $\phi(x)$. As N/κ increases, LSCF theory gives the typical parabolic density profile (which is more pronounced for larger N) with a depletion zone near the grafting substrate and an exponentially decaying tail at large x, both of which are well understood. The density profiles from canonical-ensemble simulations, however, are flatter than the LSCF predictions due to the fluctuations, which make the chains more stretched. This is shown in Figure 3a,b at $N/\kappa = 12.5$ and 125, respectively, and is also found in the toy models of $N = 3$ and 4 given in the Appendix. In most cases, the largest deviation in $\phi(x)$, defined as $\max_{\{x\}} |\phi_{\mathrm{FLMC}}(x) - \phi_{\mathrm{LSCF}}(x)|$ with $\phi_{\mathrm{FLMC}}(x)$ obtained from canonical-ensemble simulations and $\phi_{\mathrm{LSCF}}(x)$ from LSCF calculations, occurs at small x (e.g., at $x = 3$ or 4) where $\phi_{\mathrm{LSCF}}(x)$ is almost at its maximum, except for small n at large N/κ where it occurs at large x (e.g., at $x = 56$ for $n = 1$ and 2 at $N/\kappa = 125$).

On the other hand, the FLMC results approach the LSCF predictions with increasing n (thus C) at a given $N/\kappa > 0$, as expected. To quantitatively analyze the n-dependence of $\phi(x)$, we define $\varepsilon_\phi \equiv \{\sum_{x=1}^{L}[\phi_{\mathrm{FLMC}}(x) - \phi_{\mathrm{LSCF}}(x)]^2/L\}^{1/2}$; Figure 3c shows that $\varepsilon_\phi \propto n^{-1}$ at large n. Note that, at large N/κ (e.g., 500), ε_ϕ is nearly independent of n for small n, because the chains are almost fully stretched in FLMC simulations.

The brush height is directly related to $\phi(x)$, i.e., $h = 2\sum_{x=1}^{L}(x - 1)\phi(x)/L$. At $N/\kappa = 0$, LSCF theory gives the exact value of $h(N/\kappa{=}0) \approx 12.623$ for $N = 60$ on the 1D lattice. Figure 4a shows that, with increasing N/κ, $h_{\mathrm{LSCF}} - h(N/\kappa{=}0)$ monotonically increases from 0 to about 46.377 in the limit of $N/\kappa \to \infty$. We also see that, at small N/κ, $h_{\mathrm{LSCF}} - h(N/\kappa{=}0) \propto N/\kappa$, which is also found in the toy models given in the Appendix.

Figure 4b shows $h_{\mathrm{FLMC}} - h_{\mathrm{LSCF}}$ as a function of N/κ for systems with various n, where we see at least three regions of different behaviors: $h_{\mathrm{FLMC}} - h_{\mathrm{LSCF}} \propto [(N/\kappa)/\ln(N/\kappa)]^{-1}$ at large N/κ (Figure 4c) and $h_{\mathrm{FLMC}} - h_{\mathrm{LSCF}} \propto N/\kappa$ at intermediate N/κ (e.g., within [5, 30]); the former is also found in the toy models given in the Appendix. Also, at small N/κ, we see faster decrease of $h_{\mathrm{FLMC}} - h_{\mathrm{LSCF}}$ toward 0 with decreasing N/κ than in the intermediate region; this is because $h_{\mathrm{FLMC}} < h_{\mathrm{LSCF}}$ at very small $N/\kappa > 0$, as shown in Figure 4d. While LSCF theory gives the exact h at $N/\kappa = 0$, enumeration shows that $h_{\mathrm{FLMC}} < h_{\mathrm{LSCF}}$ occurs at very small N/κ for $N \geq 5$ on the 1D lattice. LSCF theory therefore overestimates h at very small $N/\kappa > 0$ (for $N \geq 5$ on the 1D lattice) and underestimates it at larger N/κ. On the other hand, in the limit of $N/\kappa \to \infty$, the system is in the ground state with all chains fully stretched, and LSCF theory becomes exact in all aspects as there are no fluctuations or correlations. This is different from the homogeneous melts studied in paper 1.[65]

3.2.2. Free-End Distribution and Chain Dimensions. Consistent with $\phi(x)$, at $N/\kappa = 0$ the ensemble-averaged free-end distribution $\phi_{s=N}(x)$ from our canonical-ensemble simulations coincides completely with the LSCF prediction (data not shown). Parts a and b of Figure 5 show $\phi_{s=N}(x)$ at $N/\kappa = 12.5$ and 125, respectively, along with the corresponding LSCF predictions; note that $\phi_{s=N}(x) = 0$ at odd x for chains of even N on the 1D lattice, and we omit such points in the figures. We see that, well inside the brush, $\phi_{s=N}(x) \propto \exp(kx/L)$, which is more pronounced for systems with smaller n at larger N/κ. This exponential distribution of the free ends can be partially attributed to the fact that the lowest-energy system configuration with one free end at $x < N$ is the one where only one chain is in the conformation of a straight rod with its last $(N - x)/2$ (which is an integer) segments folded back and all other chains are fully stretched; this configuration has an energy level $E = N - x$. Such configurations result in an exponential distribution of free ends with $k = N/2n\kappa$, when other system configurations are ignored. As shown in Figure 5c, this prediction works better for smaller n and larger N/κ. On the other hand, at given $N/\kappa > 0$, we find that $\{\sum_{x=1}^{L}[\phi_{s=N,\mathrm{FLMC}}(x) - \phi_{s=N,\mathrm{LSCF}}(x)]^2/L\}^{1/2} \propto n^{-1}$ at large n (data not shown), as in the case of $\phi(x)$.

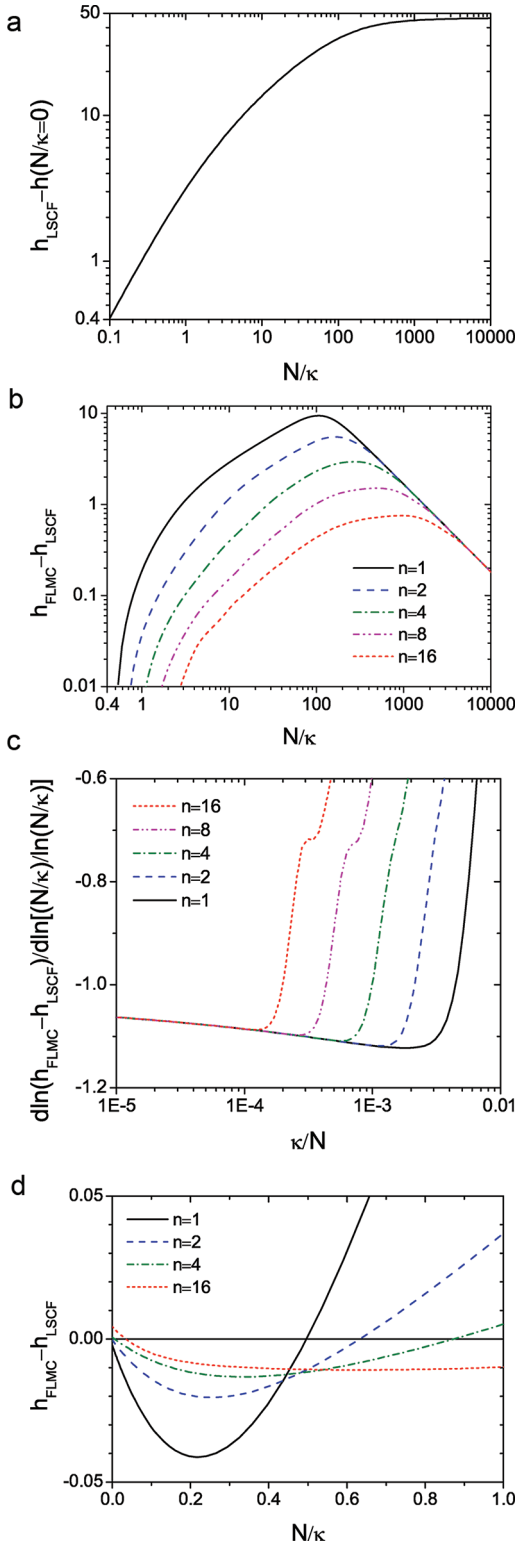

Figure 4. log−log plots of (a) the difference between the brush height obtained from LSCF theory, h_{LSCF}, and the exact value in the ideal state, $h(N/\kappa=0)$, and (b) the difference between the brush height obtained from WL-TM simulations, h_{FLMC}, and h_{LSCF} as functions of N/κ. (c) shows the scaling exponent of $h_{FLMC} - h_{LSCF}$ with $(N/\kappa)/\ln(N/\kappa)$ at $N/\kappa > 100$, obtained from the numerical differentiation of the data in part (b). (d) shows the behavior of $h_{FLMC} - h_{LSCF}$ at very small N/κ; that $h_{FLMC} \neq h_{LSCF}$ at $N/\kappa = 0$ is due to the sampling errors in WL-TM simulations.

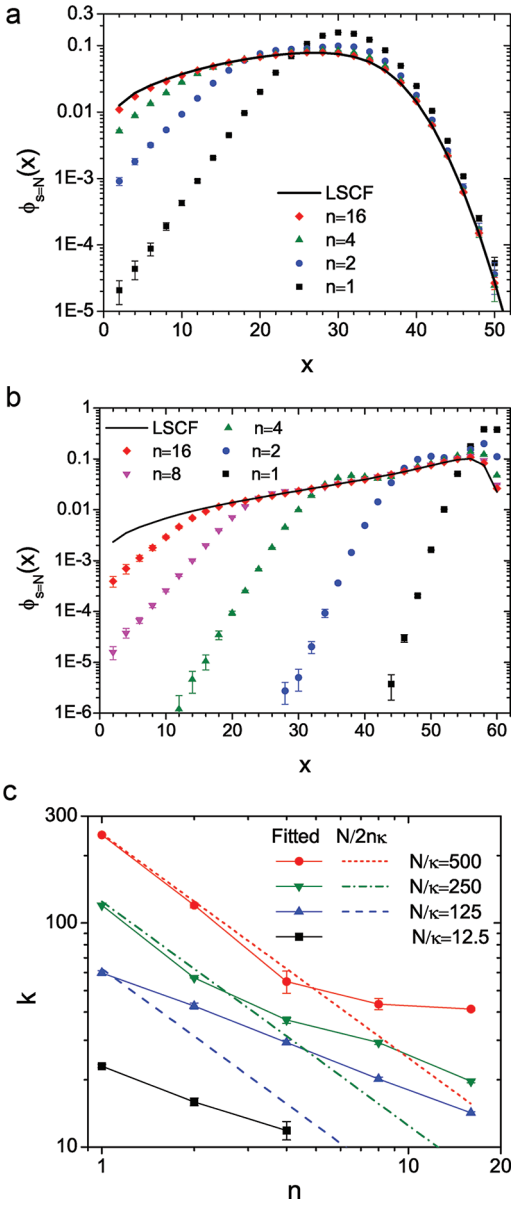

Figure 5. Free-end distributions $\phi_{s=N}(x)$ obtained from canonical-ensemble simulations on the 1D lattice with various n and the corresponding LSCF predictions at (a) $N/\kappa = 12.5$ and (b) $N/\kappa = 125$. Note that $\phi_{s=N}(x) = 0$ at odd x and we omit such points. (c) compares the k values obtained from the unweighed least-squares fit of $\phi_{s=N}(x) \propto \exp(kx/L)$ at small x with the prediction of $k = N/2n\kappa$.

The mean-square chain end-to-end distance in the x direction R_e^2 is directly related to $\phi_{s=N}(x)$, i.e., $R_e^2 = \Sigma_{x=1}^{L}(x-1)^2\phi_{s=N}(x)$. We find that both R_e^2 and the mean-square chain radius of gyration in the x direction R_g^2 exhibit qualitatively the same behavior as h. That is, LSCF theory gives exact $R_e^2 \approx 101.5$ and $R_g^2 \approx 10.98$ at $N/\kappa = 0$ for $N = 60$ on the 1D lattice. With increasing N/κ, $R_{e,LSCF}^2$ and $R_{g,LSCF}^2$ monotonically increase toward 3481 and 299.92, respectively, in the limit of $N/\kappa \rightarrow \infty$. At small N/κ, both $R_{e,LSCF}^2 - R_e^2(N/\kappa = 0)$ and $R_{g,LSCF}^2 - R_g^2(N/\kappa = 0) \propto N/\kappa$, which are also found in the toy models given in the Appendix. Furthermore, both $R_{e,FLMC}^2 - R_{e,LSCF}^2$ and $R_{g,FLMC}^2 - R_{g,LSCF}^2$ are negative at very small $N/\kappa > 0$ for $N \geq 4$ on the 1D lattice and then become positive as N/κ increases,

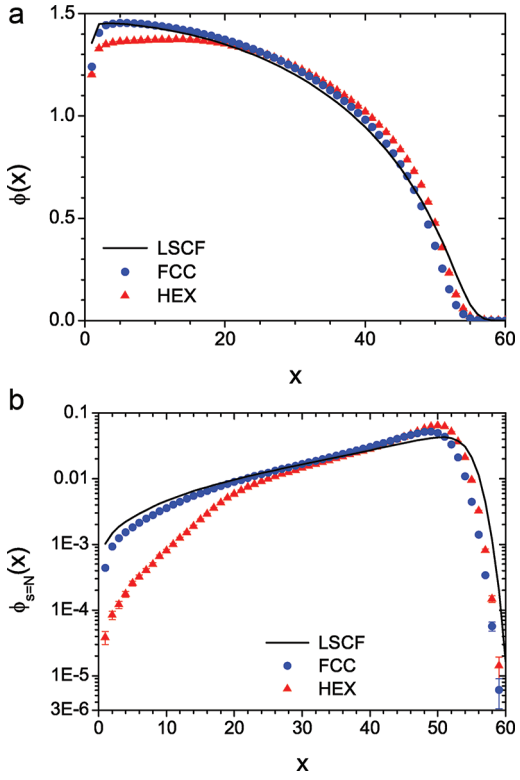

Figure 6. (a) Polymer segmental density profiles $\phi(x)$ and (b) free-end distributions $\phi_{s=N}(x)$ obtained from canonical-ensemble simulations on the 2D hexagonal (HEX) and 3D face-centered cubic (FCC) lattices at $N/\kappa = 125$, along with the corresponding LSCF predictions.

and they $\propto N/\kappa$ at intermediate N/κ and $\propto[(N/\kappa)/\ln(N/\kappa)]^{-1}$ at large N/κ (data not shown); the last scaling is also found in the toy models given in the Appendix.

3.2.3. 2D and 3D Simulations. The above FLMC results are obtained on the 1D lattice. We have also performed canonical-ensemble simulations on various 2D and 3D lattices with $L_b = 16$, which is large enough for $N = 60$. Because we use $n = L_b^{d-1}$ in these simulations, they have the same C-value as the single-chain system on the 1D lattice. Due to the quickly increased number of micro/macrostates in 2D and 3D, it becomes computationally much more expensive to obtain good estimates of DoS via WL-TM simulations; we therefore do not perform such simulations here.

Parts a and b of Figure 6 show $\phi(x)$ and $\phi_{s=N}(x)$, respectively, obtained from the canonical-ensemble simulations at $N/\kappa = 125$ on the 2D HEX and 3D FCC lattices, along with the corresponding LSCF predictions; because HEX and FCC lattices have the same $z_0 = 1/3$, the LSCF results are identical for these two lattices and different from those on the 1D lattice shown in Figures 3b and 5b. We again see that the fluctuations make the chains more stretched, i.e., that the density profiles from FLMC simulations are flatter than the LSCF predictions. The FLMC results, however, are closer to the LSCF predictions and the chains are less stretched in the x direction in higher dimensions; these are also supported by h, R_g^2, and R_e^2 data (not shown). Furthermore, $\phi_{s=N}(x)$ is no longer 0 at odd x due to $z_0 \neq 0$, and the exponential distribution of the free ends is no longer seen in 2D and 3D; the latter is also confirmed by our simulations on the 3D BCC lattice with $z_0 = 0$ (data not shown). In all the cases, however, it is clear that $\phi_{s=N,\mathrm{FLMC}}(x) < \phi_{s=N,\mathrm{LSCF}}(x)$ well inside the brush. Finally, in parts a and b of Figure 6, there is a small region at the brush tail where $\phi(x)$ and $\phi_{s=N}(x)$ from FLMC simulations are smaller than the corresponding LSCF predictions; while such a region is not seen in Figures 3b and 5b, its existence depends on the lattice and N/κ. Similar results are also found at $N/\kappa = 250$ and thus not shown.

3.3. Thermodynamic Quantities. *3.3.1. Internal Energy.* Figure 7a shows how the LSCF predictions of $E_{\mathrm{LSCF}}/{\rho_0}^2 \equiv \sum_{x=1}^{L}[{\phi_{\mathrm{LSCF}}}^2(x) - 1]$ and the directly related internal energy per chain $\beta u_{c,\mathrm{LSCF}} = (1/2N)(N/\kappa)E_{\mathrm{LSCF}}/{\rho_0}^2$ vary with N/κ. At $N/\kappa = 0$, LSCF theory gives $E_{\mathrm{LSCF}}/{\rho_0}^2 \approx 208.95$ for $N = 60$ on the 1D lattice and $\beta u_{c,\mathrm{LSCF}} = 0$, both of which are exact. In the limit of $N/\kappa \rightarrow \infty$, it also gives the exact results of 0 for both quantities. At finite $N/\kappa > 0$, while $E_{\mathrm{LSCF}}/{\rho_0}^2$ monotonically decreases with increasing N/κ, $\beta u_{c,\mathrm{LSCF}}$ exhibits a maximum around $N/\kappa \approx 66.6$. Furthermore, $\beta u_{c,\mathrm{LSCF}} \propto N/\kappa$ at small N/κ and $\beta u_{c,\mathrm{LSCF}} \propto \ln^2(N/\kappa)(N/\kappa)^{-1}$ at large N/κ; these scalings are also found in the toy models given in the Appendix. The inset of Figure 7a shows the exponent k in the corresponding scaling of $E_{\mathrm{LSCF}}/{\rho_0}^2 \propto [(N/\kappa)/(\ln N/\kappa)]^k$ at $N/\kappa \geq 200$, obtained from the numerical differentiation of the data in Figure 7a.

Figure 7b shows $(\langle E\rangle - E_{\mathrm{LSCF}})/{\rho_0}^2$ as a function of N/κ for systems with various n, where $\langle E\rangle$ is obtained from WL-TM simulations. In all the cases, $\langle E\rangle - E_{\mathrm{LSCF}}$ is positive at $N/\kappa = 0$ and exhibits a negative minimum with increasing N/κ before approaching 0 in the limit of $N/\kappa \rightarrow \infty$. To understand this behavior, we split $(\langle E\rangle - E_{\mathrm{LSCF}})/{\rho_0}^2$ into two parts: $\Delta\phi_1 \equiv \sum_{x=1}^{L}[\langle{\hat{\rho}_{\mathrm{FLMC}}}^2(x)\rangle/{\rho_0}^2 - {\phi_{\mathrm{FLMC}}}^2(x)]$ is the fluctuations of local segmental densities around their average in FLMC simulations, and $\Delta\phi_2 \equiv \sum_{x=1}^{L}[{\phi_{\mathrm{FLMC}}}^2(x) - {\phi_{\mathrm{LSCF}}}^2(x)]$ is the difference between the square of the ensemble-averaged density profile in FLMC simulations and the corresponding LSCF prediction. Both parts are due to the fluctuation effects ignored in LSCF theory.

Figure 7c shows that $\Delta\phi_1$ is always positive (at finite n and N/κ). In fact, its behavior is qualitatively the same as its equivalent in the homogeneous melts, $\langle E\rangle/{\rho_0}^2$, shown in Figure 3b of paper 1,[65] and can be understood accordingly. In particular, $\Delta\phi_1 \propto n^{-1}$ at $N/\kappa = 0$ because the chains are uncorrelated. $\Delta\phi_1$ decreases monotonically toward 0 with increasing N/κ. It also decreases monotonically toward 0 with increasing n at small $N/\kappa > 0$ but exhibits a maximum at large N/κ, the location of which increases with increasing N/κ. Finally, $\Delta\phi_1 \propto n^{-1}$ for large n at $N/\kappa > 0$; this is because the excluded-volume interactions are strongly screened as n becomes large, which makes chains less correlated, thus approaching the behavior at $N/\kappa = 0$.[65]

Figure 7d shows that $\Delta\phi_2$ is always negative at $N/\kappa > 0$ and $\propto n^{-1}$ at large n. Its behavior is qualitatively the same as ε_ϕ shown in Figure 3c (apart from the opposite sign), because both measure the difference between $\phi_{\mathrm{FLMC}}(x)$ and $\phi_{\mathrm{LSCF}}(x)$. $\Delta\phi_2$ is the fluctuation effect not present in the homogeneous melts studied in paper 1;[65] in other words, fluctuations in an inhomogeneous system can change the ensemble-averaged segmental density profile, as clearly shown in Figures 3a,3b and 6a. At large N/κ, $\Delta\phi_2$ dominates $(\langle E\rangle - E_{\mathrm{LSCF}})/{\rho_0}^2$, leading to its negative values.

Once we understand the behavior of $(\langle E\rangle - E_{\mathrm{LSCF}})/{\rho_0}^2$, it is then easy to see why LSCF theory underestimates βu_c at small N/κ and overestimates it at large N/κ, as shown in Figure 7e. We further note that $\beta(u_{c,\mathrm{FLMC}} - u_{c,\mathrm{LSCF}}) \propto N/\kappa$ at small N/κ and $\beta(u_{c,\mathrm{FLMC}} - u_{c,\mathrm{LSCF}}) \propto \ln^2(N/\kappa)(N/\kappa)^{-1}$ at large N/κ; these scalings are also found in the toy models given in the Appendix. Finally, at small and large N/κ (i.e., not close to the finite values of $N/\kappa > 0$ at which $\beta(u_{c,\mathrm{FLMC}} - u_{c,\mathrm{LSCF}}) = 0$), $\beta(u_{c,\mathrm{FLMC}} - u_{c,\mathrm{LSCF}}) \propto n^{-1}$ at large n.

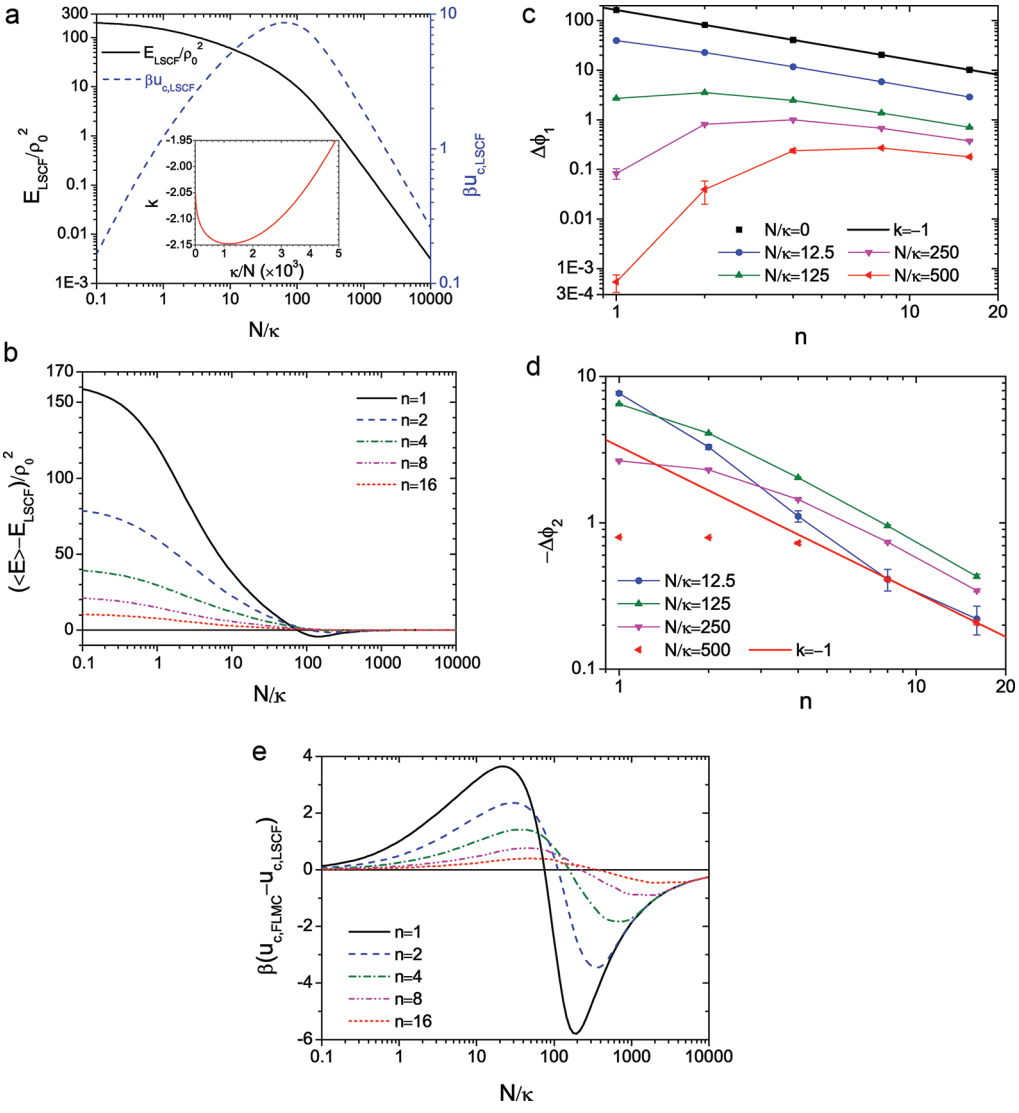

Figure 7. (a) LSCF predictions of the energy level $E_{LSCF}/\rho_0{}^2$ and the internal energy per chain $\beta u_{c,LSCF}$, where the inset shows $k \equiv \mathrm{d}\ln(E_{LSCF}/\rho_0{}^2)/\mathrm{d}\ln[(N/\kappa)/\ln(N/\kappa)]$. (b) Difference in the ensemble-averaged energy level $\langle E\rangle/\rho_0{}^2$ between WL-TM and LSCF results. (c) Fluctuations of local segmental densities around their average in canonical-ensemble simulations, $\Delta\phi_1$, where "$k = -1$" denotes a straight line of slope -1 obtained from the unweighed least-squares fit using the data points at $N/\kappa = 0$. (d) Difference between the square of the ensemble-averaged density profile in canonical-ensemble simulations and the corresponding LSCF prediction, $\Delta\phi_2$, where "$k = -1$" denotes a straight line of slope -1. (e) Difference in the internal energy per chain between WL-TM and LSCF results, $\beta(u_{c,FLMC} - u_{c,LSCF})$.

3.3.2. Free Energy and Entropy. As in paper 1,[65] here we compare the differences in free energy per chain, $\Delta f_c \equiv f_c(N/\kappa) - f_c(N/\kappa = 0)$, and in entropy per chain, $\Delta s_c \equiv s_c(N/\kappa) - s_c(N/\kappa = 0)$, from the ideal reference state at $N/\kappa = 0$, where chains do not interact with each other. Note that our SCF theory gives exact f_c and s_c both at $N/\kappa = 0$ and in the limit of $N/\kappa \to \infty$.

Figure 8a shows that the LSCF predictions of $\beta\Delta f_{c,LSCF}$ and $-\Delta s_{c,LSCF}/k_B$ both increase monotonically with increasing N/κ toward a constant $\ln(GQ^{id}) \approx 38.62$ in the limit of $N/\kappa \to \infty$ for $N = 60$ on the 1D lattice. At small N/κ, however, $\beta\Delta f_{c,LSCF} \propto N/\kappa$ while $-\Delta s_{c,LSCF}/k_B \propto (N/\kappa)^2$; these are also found in the toy models given in the Appendix.

Figure 8b shows that, at finite n and $N/\kappa > 0$, $\beta(\Delta f_{c,FLMC} - \Delta f_{c,LSCF})$ is always positive and exhibits a maximum, the location of which increases while the value decreases with increasing n. Furthermore, $\beta(\Delta f_{c,FLMC} - \Delta f_{c,LSCF}) \propto N/\kappa$ at small N/κ and $\beta(\Delta f_{c,FLMC} - \Delta f_{c,LSCF}) \propto \ln^2(N/\kappa)(N/\kappa)^{-1}$ at large N/κ; these are also found in the toy models given in the Appendix. On the other hand, Figure 8c shows that $\beta(\Delta f_{c,FLMC} - \Delta f_{c,LSCF}) \propto n^{-1}$ at large n. We also note that $\beta(\Delta f_{c,FLMC} - \Delta f_{c,LSCF})$ is nearly independent of n for small n at large N/κ (e.g., 1000), where the chains are almost fully stretched in FLMC simulations.

Finally, Figure 8d shows that $-(\Delta s_{c,FLMC} - \Delta s_{c,LSCF})/k_B$ behaves similarly to $\beta(\Delta f_{c,FLMC} - \Delta f_{c,LSCF})$, except that it is proportional to $(N/\kappa)^2$ at small N/κ; at large N/κ, we again have $-(\Delta s_{c,FLMC} - \Delta s_{c,LSCF})/k_B \propto \ln^2(N/\kappa)(N/\kappa)^{-1}$. The latter is also found in the toy models given in the Appendix. We also note that $-(\Delta s_{c,FLMC} - \Delta s_{c,LSCF})/k_B \propto n^{-1}$ at large n and that $-(\Delta s_{c,FLMC} - \Delta s_{c,LSCF})/k_B$ is nearly independent of n for small n at large N/κ (data not shown), again similar to the behavior of $\beta(\Delta f_{c,FLMC} - \Delta f_{c,LSCF})$.

dx.doi.org/10.1021/ma201310e |*Macromolecules* 2011, 44, 7837–7852

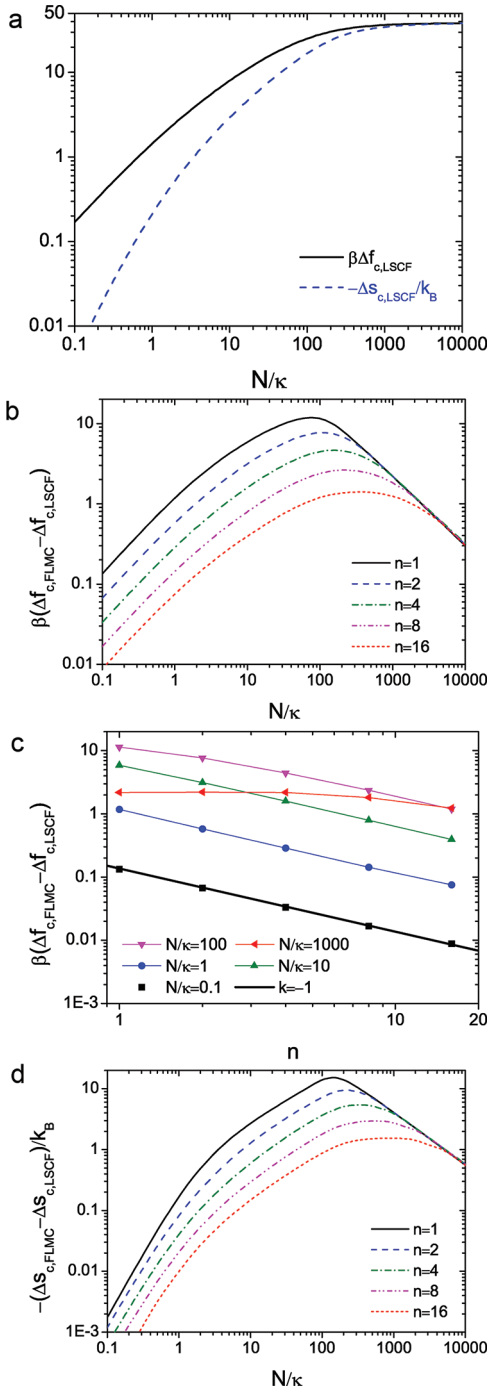

Figure 8. (a) LSCF predictions of the difference in free energy per chain, $\beta\Delta f_c$, and that in entropy per chain, $\Delta s_c/k_B$, from the ideal reference state at $N/\kappa = 0$. (b) Difference in free energy per chain between WL-TM and LSCF results, $\beta(\Delta f_{c,FLMC} - \Delta f_{c,LSCF})$, as a function of N/κ. (c) $\beta(\Delta f_{c,FLMC} - \Delta f_{c,LSCF})$ as a function of n, where "$k = -1$" denotes a straight line of slope -1 obtained from the unweighed least-squares fit using the data points at $N/\kappa = 0.1$. (d) Difference in entropy per chain between WL-TM and LSCF results, $(\Delta s_{c,FLMC} - \Delta s_{c,LSCF})/k_B$.

4. SUMMARY

Using fast lattice Monte Carlo (FLMC) simulations[64] both in a canonical ensemble and with Wang-Landau−transition-matrix (WL-TM) sampling,[69−71] we have studied a model system of homopolymer brushes in an implicit, good solvent with Kronecker δ-function interactions. The fluctuations and chain correlations in this system are controlled by two physical parameters: the chain number density $C \equiv n/V$, where n is the number of chains and V is the total number of lattice sites, and N/κ, where N is the number of segments on a chain and κ denotes the solvent quality (inversely proportional to the second virial coefficient ν). Direct comparisons of the simulation results with those from the corresponding lattice self-consistent field (LSCF) theory, both of which are based on the *same* Hamiltonian (thus without any parameter-fitting between them), unambiguously and quantitatively reveal the fluctuations and correlations in the system. This is the second paper in our series of studies with similar methodology and purpose. In our first paper (referred to as paper 1), we quantified the fluctuation/correlation effects in the corresponding homogeneous system of compressible homopolymer melts (or equivalently, homopolymers in an implicit, good solvent),[65] and the results there have helped us understand the more complex, inhomogeneous system studied in this work. Such direct comparisons distinguish our work from all previously reported comparisons between SCF theories and molecular simulations of homopolymer brushes,[15,40,41,43−45,50,52,53,58,60,62] where different models were used in the theories and simulations and thus the model differences were mixed with the consequences of the mean-field approximation (and in most cases also with those of the classical approximation and the infinite-stretching assumption) used in the SCF theories.

As in paper 1, we have first analyzed the error in our estimated free energy per chain $\beta f_{c,FLMC}$, ε_f defined in eq 27, and found that ε_f decreases monotonically with increasing N/κ. We can therefore well control the sampling error in our simulations by monitoring the error in $\beta f_{c,FLMC}(N/\kappa=0)$. We have then examined in detail how C and N/κ affect both the brush structures (i.e., the ensemble-averaged segmental density profile $\phi(x)$ and free-end distribution $\phi_{s=N}(x)$, where x denotes the direction perpendicular to the grafting substrate, as well as the related brush height h, mean-square chain end-to-end distance R_e^2 and radius of gyration R_g^2 in the x direction) and various thermodynamic quantities (i.e., the ensemble-averaged energy level $\langle E\rangle$ and related internal energy per chain u_c, the difference in free-energy per chain $\Delta f_c \equiv f_c(N/\kappa) - f_c(N/\kappa=0)$ and that in entropy per chain $\Delta s_c \equiv s_c(N/\kappa) - s_c(N/\kappa=0)$ from the ideal reference state at $N/\kappa = 0$). Such thermodynamic quantities were not examined in previous comparisons of homopolymer brushes. While most of our FLMC simulations are performed on a 1D lattice, we have also used various 2D and 3D lattices, where one chain is grafted at every lattice site at $x = 1$, ensuring the lateral homogeneity of our brushes. Our FLMC results can therefore be directly compared with the corresponding 1D LSCF calculations to reveal the effects of fluctuations and correlations in the system.

For systems at finite C, we find that LSCF theory gives exact results for all the above quantities both at $N/\kappa = 0$ and in the limit of $N/\kappa \to \infty$. In the former case, this is due to the fact that there is no chain correlations and LSCF theory includes all possible chain conformations. LSCF theory, however, gives incorrect $\langle E^2\rangle - \langle E\rangle^2 = 0$ as it neglects the system fluctuations; this is also found in paper 1.[65] In the latter case, the system is in the ground state of $E = 0$ (i.e., no fluctuations) with all chains having the same conformation (i.e., no correlations), and LSCF theory is exact in all aspects; this is different from the homogeneous melts studied in paper 1.[65]

At finite C and $N/\kappa > 0$, the segmental density profile obtained from FLMC simulations $\phi_{\mathrm{FLMC}}(x)$ is flatter than the LSCF prediction $\phi_{\mathrm{LSCF}}(x)$. The largest deviation between the two profiles occurs in most cases close to the grafting substrate, where $\phi_{\mathrm{LSCF}}(x)$ is almost at its maximum. The profile differences, however, are smaller in higher dimensions. For small n and large N/κ, our 1D simulations also show an exponential distribution of the free ends well inside the brush, which is not found in 2D and 3D simulations nor in LSCF predictions. In all the cases, however, the free-end density from FLMC simulations $\phi_{s=N,\mathrm{FLMC}}(x)$ is lower than the LSCF prediction $\phi_{s=N,\mathrm{LSCF}}(x)$ well inside the brush. As for h, we find that $h_{\mathrm{LSCF}} - h(N/\kappa = 0) \propto N/\kappa$ at small N/κ, and that $h_{\mathrm{FLMC}} - h_{\mathrm{LSCF}} \propto N/\kappa$ at intermediate N/κ (e.g., within [5, 30]) and $h_{\mathrm{FLMC}} - h_{\mathrm{LSCF}} \propto \ln(N/\kappa)(N/\kappa)^{-1}$ at large N/κ. These behaviors are also found in ${R_e}^2$ and ${R_g}^2$.

Regarding the thermodynamic quantities, LSCF theory predicts that $\beta u_{c,\mathrm{LSCF}} = 0$ both at $N/\kappa = 0$ and in the limit of $N/\kappa \rightarrow \infty$, and that $\beta u_{c,\mathrm{LSCF}} \propto N/\kappa$ at small N/κ and $\beta u_{c,\mathrm{LSCF}} \propto \ln^2(N/\kappa)(N/\kappa)^{-1}$ at large N/κ. Furthermore, $\beta \Delta f_{c,\mathrm{LSCF}}$ and $-\Delta s_{c,\mathrm{LSCF}}/k_B$ both increase monotonically with increasing N/κ toward a finite constant in the limit of $N/\kappa \rightarrow \infty$. At small N/κ, however, $\beta \Delta f_{c,\mathrm{LSCF}} \propto N/\kappa$ while $-\Delta s_{c,\mathrm{LSCF}}/k_B \propto (N/\kappa)^2$.

For our model system, $\langle E \rangle / {\rho_0}^2 = 2N\beta u_c/(N/\kappa)$ is directly related to $\phi(x)$, where the average segmental density $\rho_0 = CN$. We can therefore split $(\langle E \rangle - E_{\mathrm{LSCF}})/{\rho_0}^2$ into two parts: $\Delta\phi_1$ is the fluctuations of local segmental densities around their average in FLMC simulations, and $\Delta\phi_2$ is the difference between the square of the ensemble-averaged density profile in FLMC simulations and the corresponding LSCF prediction. Both parts are due to the fluctuation effects ignored in LSCF theory, and $\Delta\phi_2$ is unique for inhomogeneous systems. We find that $\Delta\phi_1$ is always positive (at finite C and N/κ) and has qualitatively the same behavior as its equivalent in the homogeneous melts studied in paper 1,[65] and that $\Delta\phi_2$ is always negative (at finite C and $N/\kappa > 0$) and dominates $(\langle E \rangle - E_{\mathrm{LSCF}})/{\rho_0}^2$ at large N/κ. This explains why LSCF theory underestimates βu_c of the brushes at small N/κ and overestimates it at large N/κ. In addition, we find that $\beta(u_{c,\mathrm{FLMC}} - u_{c,\mathrm{LSCF}}) \propto N/\kappa$ at small N/κ and $\beta(u_{c,\mathrm{FLMC}} - u_{c,\mathrm{LSCF}}) \propto \ln^2(N/\kappa)(N/\kappa)^{-1}$ at large N/κ.

On the other hand, at finite C and $N/\kappa > 0$, $\beta(\Delta f_{c,\mathrm{FLMC}} - \Delta f_{c,\mathrm{LSCF}})$ is always positive and exhibits a maximum, the location of which increases while the value decreases with increasing C. Furthermore, $\beta(\Delta f_{c,\mathrm{FLMC}} - \Delta f_{c,\mathrm{LSCF}}) \propto N/\kappa$ at small N/κ and $\beta(\Delta f_{c,\mathrm{FLMC}} - \Delta f_{c,\mathrm{LSCF}}) \propto \ln^2(N/\kappa)(N/\kappa)^{-1}$ at large N/κ. $-(\Delta s_{c,\mathrm{FLMC}} - \Delta s_{c,\mathrm{LSCF}})/k_B$ behaves similarly to $\beta(\Delta f_{c,\mathrm{FLMC}} - \Delta f_{c,\mathrm{LSCF}})$, except that it is proportional to $(N/\kappa)^2$ at small N/κ.

Finally, at given $N/\kappa > 0$, FLMC results approach LSCF predictions at a rate of $1/C$ at large C. This scaling has also been found in our previous work.[64,65] As expected, LSCF theory is exact in the limit of $C \rightarrow \infty$, where there are no fluctuations or correlations. For the homopolymer brushes studied here, however, this scaling does not hold for certain quantities close to the finite values of N/κ at which the FLMC results concide with LSCF predictions, e.g., $\langle E \rangle$ and βu_c at intermediate N/κ (Figure 7b,d).

It is interesting to note that most of the above results are also found in the toy models of $N = 3$ and 4 in 1D and 2D given in the Appendix. While the corrections to LSCF results at small N/κ are captured by a lattice Gaussian fluctuation theory, which is analogous to that presented in our paper 1[65] and will be reported in a later paper in our series, to the best of our knowledge, so far no theory explains our corrections at large N/κ. We thus hope that this work will promote the development of advanced theories that include these identified fluctuation/correlation effects. We also note that homopolymer brushes in an explicit solvent with varying quality are examined in a subsequent paper in our series.[66]

APPENDIX

Here we give the analytical results for brushes of $N = 3$ and 4 in 1D, as well as those for laterally homogeneous brushes of $N = 3$ in 2D on the square lattice, which in most cases have the same scalings as found for larger N in the main text.

A. $N = 3$ in 1D. Consider n grafted chains each of $N = 3$ segments. There are only two possible conformations for a grafted chain: (I) $X_1 = 1$, $X_2 = 2$, and $X_3 = 3$ and (II) $X_1 = 1$, $X_2 = 2$, and $X_3 = 1$, where X_s denotes the position of the sth segment on the chain. The total number of system configurations (density of states) with i chains in conformation I and $n - i$ chains in conformation II (referred to as energy level i) is $\Omega_i = 1/i!(n-i)!$, and we have $\sum_{i=0}^{n}\Omega_i = 2^n/n!$ (note that the chains are indistinguishable). For energy level i, the normalized segmental density at position x, denoted by $\phi_{x,i} \equiv \hat{\rho}_i(x)/\rho_0$ with $\hat{\rho}_i(x)$ being the microscopic segmental density at x, is then $\phi_{1,i} = 2 - i/n$, $\phi_{2,i} = 1$, and $\phi_{3,i} = i/n$, and the corresponding system Hamiltonian due to nonbonded interactions is $\beta\mathscr{H}_i^E = (n/3)(N/\kappa)(1 - i/n)^2$. The canonical-ensemble partition function is $\mathscr{Z} = \sum_{i=0}^{n}\Omega_i \exp(-\beta\mathscr{H}_i^E)$, and the normalized probability of energy level i is $P_i = \Omega_i \exp(-\beta\mathscr{H}_i^E)/\mathscr{Z}$ with $\sum_{i=0}^{n}P_i = 1$. Using ϕ_x as a shorthand notation of $\phi(x)$, we therefore have

$$\phi_1 = \sum_{i=0}^{n} P_i\phi_{1,i} = 2 - \frac{\langle i \rangle}{n} \qquad \phi_2 = 1 \qquad \phi_3 = 2 - \phi_1$$

$$h = \frac{10 - 4\phi_1}{3} \qquad {R_e}^2 = 8 - 4\phi_1 \qquad {R_g}^2 = \frac{10 - 4\phi_1}{9}$$

$$\frac{\langle E \rangle}{{\rho_0}^2} = 2 - \frac{4\langle i \rangle}{n} + \frac{2\langle i^2 \rangle}{n^2} \qquad \beta u_c = \frac{N}{6\kappa}\frac{\langle E \rangle}{{\rho_0}^2}$$

$$\beta\Delta f_c(N/\kappa) \equiv -\frac{1}{n}\ln\frac{\mathscr{Z}(N/\kappa)}{\mathscr{Z}(N/\kappa = 0)} = \ln 2 - \frac{1}{n}\ln\sum_{i=0}^{n}\frac{n!}{i!(n-i)!}\exp\left[-\frac{n}{3}\frac{N}{\kappa}\left(1 - \frac{i}{n}\right)^2\right] \quad (29)$$

In the limit of $n \rightarrow \infty$, the system is dominated by a single energy level i^* having the maximum P_{i^*}, i.e., $(\partial \ln P_i/\partial i)|_{i=i^*} = 0$. With the Stirling approximation $\ln n! \approx n \ln n - n$, this gives

$$\ln\frac{p}{1-p} = \frac{2}{3}\frac{N}{\kappa}(1-p) \quad (30)$$

where $p \equiv i^*/n$. Substituting $\phi_1^* = 2 - p$ into eq 30, we obtain

$$\phi_1^* = 1 + \left\{1 + \exp\left[\frac{2}{3}\frac{N}{\kappa}(\phi_1^* - 1)\right]\right\}^{-1} \quad (31)$$

It is easy to show that eq 31 is the same as the LSCF equations, eqs 12−14, for $N = 3$; LSCF theory is therefore exact in the limit of $n \rightarrow \infty$. Hereafter we use "*" to denote LSCF results. We further have

$$\frac{E^*}{{\rho_0}^2} = 2(1-p)^2 \qquad \beta u_c^* = \frac{N}{3\kappa}(1-p)^2 \quad (32)$$

and with the Stirling approximation

$$\beta\Delta f_c^* = \ln 2 + \frac{1+p}{2}\ln p + \frac{1-p}{2}\ln(1-p) \quad (33)$$

From eq 30, it is clear that $p(N/\kappa=0) = 1/2$, $\lim_{N/\kappa\to\infty} p = 1$ (i.e., all chains are fully stretched and thus in conformation I), and $\lim_{N/\kappa\to\infty} \beta u_c^* = (1/2)\lim_{p\to 1}(1-p)\ln(p/(1-p)) = 0$; we also have $\lim_{N/\kappa\to\infty} \beta\Delta f_c^* = \ln 2$. Furthermore, at small N/κ, Taylor-expanding eq 30 gives $p \approx 1/2 + N/12\kappa - (1/72)(N/\kappa)^2$, and thus

$$\phi_1^* - \phi_1(N/\kappa=0) \approx -\frac{N}{12\kappa} \tag{34}$$

$$h^* - h(N/\kappa=0) \approx \frac{N}{9\kappa} \tag{35}$$

$$R_e^{2*} - R_e^2(N/\kappa=0) \approx \frac{N}{3\kappa} \tag{36}$$

$$R_g^{2*} - R_g^2(N/\kappa = 0) \approx \frac{N}{27\kappa} \tag{37}$$

$$\frac{E^* - E(N/\kappa=0)}{\rho_0^2} \approx -\frac{N}{6\kappa} \tag{38}$$

$$\beta u_c^* \approx \frac{N}{12\kappa} \tag{39}$$

$$\beta\Delta f_c^* \approx \frac{N}{12\kappa} \tag{40}$$

$$\Delta s_c^*/k_B \approx -\frac{1}{72}\left(\frac{N}{\kappa}\right)^2 \tag{41}$$

On the other hand, at large N/κ, Taylor-expanding eq 30 gives $p \approx 1 - a(\kappa/N)$ with $a = -(3/2)(\ln a - \ln(N/\kappa))$; ignoring the $\ln a$ term gives $E^*/\rho_0^2 \approx (9/2)\ln^2(N/\kappa)(N/\kappa)^{-2}$ and $\beta u_c^* \approx (3/4)\ln^2(N/\kappa)(N/\kappa)^{-1}$.

Similarly, for $n = 1$ we have

$$\phi_1^* - \phi_1 \approx \begin{cases} \frac{1}{72}\left(\frac{N}{\kappa}\right)^2 & \text{at small } N/\kappa \\ \frac{3}{2}\left(\ln\frac{N}{\kappa}\right)\left(\frac{N}{\kappa}\right)^{-1} & \text{at large } N/\kappa \end{cases} \tag{42}$$

$$\beta(\Delta f_c - \Delta f_c^*) \approx \begin{cases} \frac{N}{12\kappa} - \frac{1}{432}\left(\frac{N}{\kappa}\right)^3 & \text{at small } N/\kappa \\ \frac{9}{4}\left(\ln\frac{N}{\kappa}\right)^2\left(\frac{N}{\kappa}\right)^{-1} & \text{at large } N/\kappa \end{cases} \tag{43}$$

$$\beta(u_c - u_c^*) \approx \begin{cases} \frac{N}{12\kappa} - \frac{1}{144}\left(\frac{N}{\kappa}\right)^3 & \text{at small } N/\kappa \\ -\frac{9}{4}\left(\ln\frac{N}{\kappa}\right)^2\left(\frac{N}{\kappa}\right)^{-1} & \text{at large } N/\kappa \end{cases} \tag{44}$$

For $n = 2$ we have

$$\phi_1^* - \phi_1 \approx \frac{1}{144}\left(\frac{N}{\kappa}\right)^2 \tag{45}$$

$$\beta(\Delta f_c - \Delta f_c^*) \approx \frac{N}{24\kappa} - \frac{1}{576}\left(\frac{N}{\kappa}\right)^2 \tag{46}$$

$$\beta(u_c - u_c^*) \approx \frac{N}{24\kappa} - \frac{1}{288}\left(\frac{N}{\kappa}\right)^2 \tag{47}$$

at small N/κ, where the scaling of $(\Delta s_c - \Delta s_c^*)/k_B = \beta[(u_c - u_c^*) - (\Delta f_c - \Delta f_c^*)]$ with N/κ is different from the $n = 1$ case; at large N/κ, the same results as in the $n = 1$ case are obtained. The limiting behaviors of $h - h^*$, $R_e^2 - R_e^{2*}$, and $R_g^2 - R_g^{2*}$ can be obtained from their linear relations with $\phi_1 - \phi_1^*$.

B. $N = 4$ in 1D. Here we have three possible conformations for a grafted chain: (I) $X_1 = 1$, $X_2 = 2$, $X_3 = 3$, and $X_4 = 4$, (II) $X_1 = 1$, $X_2 = 2$, $X_3 = 3$, and $X_4 = 2$, and (III) $X_1 = 1$, $X_2 = 2$, $X_3 = 1$, and $X_4 = 2$. The total number of system configurations (density of states) with i chains in conformation I, j chains in conformation II and $n - i - j$ chains in conformation III (referred to as energy level (i, j)) is $\Omega_{(i,j)} = 1/i!j!(n - i - j)!$, and we have $\sum_{i=0}^{n}\sum_{j=0}^{n-i}\Omega_{(i,j)} = 3^n/n!$. For energy level (i, j), we have $\phi_{1,(i,j)} = 2 - (i + j)/n$, $\phi_{2,(i,j)} = 2 - i/n$, $\phi_{3,(i,j)} = (i + j)/n$, and $\phi_{4,(i,j)} = i/n$, and the corresponding system Hamiltonian due to nonbonded interactions is $\beta\mathcal{H}^E_{(i,j)} = (n/4)(N/\kappa)[(1 - (i + j)/n)^2 + (1 - i/n)^2]$. The canonical-ensemble partition function is $\mathcal{Z} = \sum_{i=0}^{n}\sum_{j=0}^{n-i}\Omega_{(i,j)}\exp(-\beta\mathcal{H}^E_{(i,j)})$ and the normalized probability of energy level (i,j) is $P_{(i,j)} = \Omega_{(i,j)}\exp(-\beta\mathcal{H}^E_{(i,j)})/\mathcal{Z}$ with $\sum_{i=0}^{n}\sum_{j=0}^{n-i}P_{(i,j)} = 1$. We therefore have

$$\phi_1 = 2 - \frac{\langle i + j\rangle}{n} \qquad \phi_2 = 2 - \frac{\langle i\rangle}{n} \qquad \phi_3 = 2 - \phi_1$$

$$\phi_4 = 2 - \phi_2 \qquad h = 5 - \phi_1 - \phi_2 \qquad R_e^2 = 17 - 8\phi_2$$

$$R_g^2 = \frac{9 - \phi_1 - 3\phi_2}{4}$$

$$\frac{\langle E\rangle}{\rho_0^2} = 4 - \frac{\langle 8i + 4j\rangle}{n} + \frac{\langle 4i^2 + 4ij + 2j^2\rangle}{n^2}$$

$$\beta u_c = \frac{N}{8\kappa}\frac{\langle E\rangle}{\rho_0^2}$$

$$\beta\Delta f_c(N/\kappa) = \ln 3 - \frac{1}{n}\ln\sum_{i=0}^{n}\sum_{j=0}^{n-i}\frac{n!}{i!j!(n-i-j)!} \times\exp\left\{-\frac{n}{4}\frac{N}{\kappa}\left[\left(1-\frac{i+j}{n}\right)^2 + \left(1-\frac{i}{n}\right)^2\right]\right\} \tag{48}$$

In the limit $n \to \infty$, the system is dominated by a single energy level (i^*, j^*) having the maximum $P_{(i^*,j^*)}$, i.e., $(\partial \ln P_{(i,j)}/\partial i)|_{i=i^*,j=j^*} = (\partial \ln P_{(i,j)}/\partial j)|_{i=i^*,j=j^*} = 0$. With the Stirling approximation, this gives

$$\ln\frac{q}{1-p-q} = \frac{N}{2\kappa}(1-p-q) \tag{49}$$

$$\ln\frac{p}{q} = \frac{N}{2\kappa}(1-p) \tag{50}$$

where $p \equiv i^*/n$ and $q \equiv j^*/n$. It is easy to show that these are the same as the LSCF equations, eqs 12−14, for $N = 4$. We further have

$$\frac{E^*}{\rho_0^2} = 2[(1-p-q)^2 + (1-p)^2]$$

$$\beta u_c^* = \frac{N}{4\kappa}[(1-p-q)^2 + (1-p)^2] \tag{51}$$

and with the Stirling approximation

$$\beta\Delta f_c^* = \ln 3 + \frac{1+p}{2}\ln p + \frac{1-p-q}{2}\ln(1-p-q) + \frac{q}{2}\ln q \quad (52)$$

From eqs 49 and 50, it is clear that $p(N/\kappa{=}0) = q(N/\kappa{=}0) = 1/3$, $\lim_{N/\kappa\to\infty} p = 1$, $\lim_{N/\kappa\to\infty} q = 0$, and $\lim_{N/\kappa\to\infty} \beta u_c^* = (1/2)\lim_{p\to1,q\to0}[(1-p-q)\ln(q/(1-p-q)) + (1-p)\ln(p/q)] = 0$; we also have $\lim_{N/\kappa\to\infty}\beta\Delta f_c^* = \ln 3$. Furthermore, at small N/κ, Taylor-expanding eqs 49 and 50 gives $p \approx 1/3 + (5/54)N/\kappa - (17/1944)(N/\kappa)^2$ and $q \approx 1/3 - N/54\kappa - (11/1944)(N/\kappa)^2$, and thus

$$\phi_1^* - \phi_1(N/\kappa{=}0) \approx -\frac{2}{27}\frac{N}{\kappa} \quad (53)$$

$$\phi_2^* - \phi_2(N/\kappa{=}0) \approx -\frac{5}{54}\frac{N}{\kappa} \quad (54)$$

$$h^* - h(N/\kappa{=}0) \approx \frac{N}{6\kappa} \quad (55)$$

$$R_e^{2*} - R_e^2(N/\kappa{=}0) \approx \frac{20}{27}\frac{N}{\kappa} \quad (56)$$

$$R_g^{2*} - R_g^2(N/\kappa{=}0) \approx \frac{19}{216}\frac{N}{\kappa} \quad (57)$$

$$\frac{E^* - E(N/\kappa{=}0)}{\rho_0^2} \approx -\frac{28}{81}\frac{N}{\kappa} \quad (58)$$

$$\beta u_c^* \approx \frac{5}{36}\frac{N}{\kappa} \quad (59)$$

$$\beta\Delta f_c^* \approx \frac{5}{36}\frac{N}{\kappa} \quad (60)$$

$$\Delta s_c^*/k_B \approx -\frac{7}{324}\left(\frac{N}{\kappa}\right)^2 \quad (61)$$

On the other hand, at large N/κ, Taylor-expanding eqs 49 and 50 gives $p \approx 1 + a(\kappa/N)$ and $q \approx b(\kappa/N)$ with $a < 0$ and $b > 0$ satisfying the following equations (note that $a + b < 0$):

$$a = 2\ln b - 2\ln\frac{N}{\kappa} \qquad b = 2\ln[-(a+b)] - 4\ln b + 2\ln\frac{N}{\kappa} \quad (62)$$

ignoring the $\ln b$ and $\ln[-(a+b)]$ terms gives $E^*/\rho_0^2 \approx 8\ln^2(N/\kappa)(N/\kappa)^{-2}$ and $\beta u_c^* \approx \ln^2(N/\kappa)(N/\kappa)^{-1}$.

Similarly, for $n = 1$ we have

$$\phi_1^* - \phi_1 \approx \begin{cases} \dfrac{N}{108\kappa} + \dfrac{85}{7776}\left(\dfrac{N}{\kappa}\right)^2 & \text{at small } N/\kappa \\ 2\ln\left(2\ln\dfrac{N}{\kappa}\right)\left(\dfrac{N}{\kappa}\right)^{-1} & \text{at large } N/\kappa \end{cases} \quad (63)$$

$$\phi_2^* - \phi_2 \approx \begin{cases} -\dfrac{N}{108\kappa} + \dfrac{95}{7776}\left(\dfrac{N}{\kappa}\right)^2 & \text{at small } N/\kappa \\ 2\left(\ln\dfrac{N}{\kappa}\right)\left(\dfrac{N}{\kappa}\right)^{-1} & \text{at large } N/\kappa \end{cases} \quad (64)$$

$$\beta(\Delta f_c - \Delta f_c^*) \approx \begin{cases} \dfrac{N}{9\kappa} + \dfrac{1}{1296}\left(\dfrac{N}{\kappa}\right)^2 & \text{at small } N/\kappa \\ \left(\ln\dfrac{N}{\kappa}\right)^2\left(\dfrac{N}{\kappa}\right)^{-1} & \text{at large } N/\kappa \end{cases} \quad (65)$$

$$\beta(u_c - u_c^*) \approx \begin{cases} \dfrac{N}{9\kappa} + \dfrac{1}{648}\left(\dfrac{N}{\kappa}\right)^2 & \text{at small } N/\kappa \\ -\left(\ln\dfrac{N}{\kappa}\right)^2\left(\dfrac{N}{\kappa}\right)^{-1} & \text{at large } N/\kappa \end{cases} \quad (66)$$

Note that the result at large N/κ in eq 63 is obtained under the approximation $a + b \approx -2\ln b$. The limiting behaviors of $h - h^*$, $R_e^2 - R_e^{2*}$, and $R_g^2 - R_g^{2*}$ can be obtained from their linear relations with $\phi_1 - \phi_1^*$ and $\phi_2 - \phi_2^*$.

C. $N = 3$ on 2D Square Lattice. Consider n_t grafted chains each of $N = 3$ segments on 2D square lattice (SQL) with $V = NL_b$. There are totally ten different conformations for each chain, thus nine indices are needed to specify an energy level in general, which makes it difficult to obtain the analytical solution. We therefore further assume the lateral homogeneity of the brush, where $n = n_t/L_b$ chains are grafted at each lattice site at $x = 1$. The ten conformations can then be grouped into four classes: (I) $\hat\rho(x=1) = 3$, $\hat\rho(x=2) = 0$, and $\hat\rho(x=3) = 0$, (II) $\hat\rho(x{=}1) = 2$, $\hat\rho(x{=}2) = 1$, and $\hat\rho(x{=}3) = 0$, (III) $\hat\rho(x{=}1) = 1$, $\hat\rho(x{=}2) = 2$, and $\hat\rho(x{=}3) = 0$, and (IV) $\hat\rho(x{=}1) = 1$, $\hat\rho(x{=}2) = 1$, and $\hat\rho(x{=}3) = 1$. The total number of system configurations (density of states) with i chains in class I, j chains in class II, k chains in class III, and $n - i - j - k$ chains in class IV (referred to as energy level (i, j, k)) is $\Omega_{(i,j,k)} = 4^i 3^j 2^k/[i!j!k!(n-i-j-k)!]$, where 4^i is due to the fact that there are four different conformations in class I, and so on. Clearly, we have $\sum_{i=0}^{n}\sum_{j=0}^{n-i}\sum_{k=0}^{n-i-j}\Omega_{(i,j,k)} = 10^n/n!$. For energy level (i, j, k), we have $\phi_{1,(i,j,k)} = 1 + (2i+j)/n$, $\phi_{2,(i,j,k)} = 1 + (k-i)/n$, $\phi_{3,(i,j,k)} = 1 - (i+j+k)/n$, and the corresponding system Hamiltonian due to nonbonded interactions is $\beta\mathscr{H}^E_{(i,j,k)} = (1/6n)(N/\kappa)[6i^2 + 2j^2 + 2k^2 + 6ij + 2jk]$. The canonical-ensemble partition function is $\mathscr{Z} = \sum_{i=0}^{n}\sum_{j=0}^{n-i}\sum_{k=0}^{n-i-j}\Omega_{(i,j,k)}\exp(-\beta\mathscr{H}^E_{(i,j,k)})$ and the normalized probability of energy level (i, j, k) is $P_{(i,j,k)} = \Omega_{(i,j,k)}\exp(-\beta\mathscr{H}^E_{(i,j,k)})/\mathscr{Z}$ with $\sum_{i=0}^{n}\sum_{j=0}^{n-i}\sum_{k=0}^{n-i-j}P_{(i,j,k)} = 1$. We therefore have

$$\phi_1 = 1 + \frac{\langle 2i + j\rangle}{n} \qquad \phi_2 = 1 - \frac{\langle i - k\rangle}{n}$$

$$h = 4 - \frac{2}{3}(2\phi_1 + \phi_2) \qquad R_e^2 = 4 - \frac{\langle 12i + 10j + 9k\rangle}{3n}$$

$$R_g^2 = \frac{2}{3} - \frac{\langle 6i + 4j + 4k\rangle}{9n}$$

$$\frac{\langle E\rangle}{\rho_0^2} = \frac{\langle 6i^2 + 2j^2 + 2k^2 + 6ij + 2jk\rangle}{3n} \qquad \beta u_c = \frac{N}{6\kappa}\frac{\langle E\rangle}{\rho_0^2}$$

$$\beta\Delta f_c(N/\kappa) = \ln 10 - \frac{1}{n}\ln \sum_{i=0}^{n}\sum_{j=0}^{n-i}\sum_{k=0}^{n-i-j} \frac{4^i 3^j 2^k n!}{i!j!k!(n-i-j-k)!} \times \exp\left(-\frac{3i^2 + j^2 + k^2 + 3ij + jk}{3n}\frac{N}{\kappa}\right) \quad (67)$$

In the limit of $n \to \infty$, the system is dominated by a single energy level (i^*, j^*, k^*) having the maximum $P_{(i^*,j^*,k^*)}$, i.e., $(\partial \ln P_{(i,j,k)}/\partial i)|_{i=i^*,j=j^*,k=k^*} = (\partial \ln P_{(i,j,k)}/\partial j)|_{i=i^*,j=j^*,k=k^*} = (\partial \ln P_{(i,j,k)}/\partial k)|_{i=i^*,j=j^*,k=k^*} = 0$. With the Stirling approximation and a little algebra (i.e., only two of these equations are independent and $k^*/n = 9q^2/8p$), we obtain

$$\ln\frac{1-p-q-8q^2/9p}{p/4} = \frac{N}{\kappa}(2p + q) \quad (68)$$

$$\ln\frac{1-p-q-8q^2/9p}{q/3} = \frac{N}{\kappa}\left(p + \frac{2q}{3} + \frac{8q^2}{27p}\right) \quad (69)$$

where $p \equiv i^*/n$ and $q \equiv j^*/n$. It is easy to show that these are the same as the LSCF equations, eqs 12−14, for $N = 3$ on SQL (i.e., with $z_0 = 1/2$). We further have

$$\frac{E^*}{{\rho_0}^2} = 6p^2 + 2q^2 + \frac{128q^4}{81p^2} + 6pq + \frac{16q^3}{9p} \qquad \beta u_c^* = \frac{N}{6\kappa}\frac{E^*}{{\rho_0}^2} \quad (70)$$

and with the Stirling approximation

$$\beta\Delta f_c^* = \ln 10 + \frac{N}{\kappa}\left(p^2 + pq + \frac{q^2}{3} + \frac{64q^4}{243p^2} + \frac{8q^3}{27p}\right) + p\ln\frac{p}{4} + q\ln\frac{q}{3} + \frac{8q^2}{9p}\ln\frac{4q^2}{9p} + \left(1-p-q-\frac{8q^2}{9p}\right)\ln\left(1-p-q-\frac{8q^2}{9p}\right) \quad (71)$$

From eqs 68 and 69, it is clear that $p(N/\kappa{=}0) = 2/5$, $q(N/\kappa{=}0) = 3/10$, $\lim_{N/\kappa\to\infty} p = 0$, $\lim_{N/\kappa\to\infty} q = 0$, and $\lim_{N/\kappa\to\infty} \beta u_c^* = 0$; we also have $\lim_{N/\kappa\to\infty} \beta\Delta f_c^* = \ln 10$. Furthermore, at small N/κ, Taylor-expanding eqs 68 and 69 gives $p \approx 2/5 - (62/375)(N/\kappa) + (1969/28125)(N/\kappa)^2$ and $q \approx 3/10 + (3/500)(N/\kappa) - (4669/150000)(N/\kappa)^2$, and thus

$$\phi_1^* - \phi_1(N/\kappa{=}0) \approx -\frac{487}{1500}\frac{N}{\kappa} \quad (72)$$

$$\phi_2^* - \phi_2(N/\kappa{=}0) \approx \frac{32}{125}\frac{N}{\kappa} \quad (73)$$

$$h^* - h(N/\kappa{=}0) \approx \frac{59}{225}\frac{N}{\kappa} \quad (74)$$

$${R_e}^{2*} - {R_e}^2(N/\kappa{=}0) \approx \frac{277}{750}\frac{N}{\kappa} \quad (75)$$

$${R_g}^{2*} - {R_g}^2(N/\kappa{=}0) \approx \frac{227}{3375}\frac{N}{\kappa} \quad (76)$$

$$\frac{E^* - E(N/\kappa = 0)}{{\rho_0}^2} \approx -\frac{1763}{1875}\frac{N}{\kappa} \quad (77)$$

$$\beta u_c^* \approx \frac{103}{300}\frac{N}{\kappa} \quad (78)$$

$$\beta\Delta f_c^* \approx \frac{103}{300}\frac{N}{\kappa} \quad (79)$$

$$\Delta s_c^*/k_B \approx -\frac{1763}{22500}\left(\frac{N}{\kappa}\right)^2 \quad (80)$$

On the other hand, at large N/κ, Taylor-expanding eqs 68 and 69 gives $p \approx a(\kappa/N)$ and $q \approx b(\kappa/N)$ with $a > 0$ and $b > 0$ satisfying the following equations:

$$2a + b = -\ln\frac{a}{4} + \ln\frac{N}{\kappa}$$
$$3a + 2b + \frac{8b^2}{9a} = -3\ln\frac{b}{3} + 3\ln\frac{N}{\kappa} \quad (81)$$

ignoring the $\ln(a/4)$ and $\ln(b/3)$ terms gives $E^*/{\rho_0}^2 \approx 6\ln^2(N/\kappa)(N/\kappa)^{-2}$ and $\beta u_c^* \approx \ln^2(N/\kappa)(N/\kappa)^{-1}$.

Similarly, for $n = 1$ (i.e., one chain grafted at each lattice site at $x = 1$), we have

$$\phi_1^* - \phi_1 \approx \begin{cases} -\frac{6}{125}\frac{N}{\kappa} & \text{at small } N/\kappa \\ \left(\ln\frac{N}{\kappa}\right)\left(\frac{N}{\kappa}\right)^{-1} & \text{at large } N/\kappa \end{cases} \quad (82)$$

$$\phi_2^* - \phi_2 \approx \begin{cases} \frac{9}{250}\frac{N}{\kappa} & \text{at small } N/\kappa \\ \left(\ln\frac{N}{\kappa}\right)\left(\frac{N}{\kappa}\right)^{-1} & \text{at large } N/\kappa \end{cases} \quad (83)$$

$$\beta(\Delta f_c - \Delta f_c^*) \approx \begin{cases} \frac{67}{300}\frac{N}{\kappa} + \frac{167}{15000}\left(\frac{N}{\kappa}\right)^2 & \text{at small } N/\kappa \\ \left(\ln\frac{N}{\kappa}\right)^2\left(\frac{N}{\kappa}\right)^{-1} & \text{at large } N/\kappa \end{cases} \quad (84)$$

$$\beta(u_c - u_c^*) \approx \begin{cases} \frac{67}{300}\frac{N}{\kappa} + \frac{167}{7500}\left(\frac{N}{\kappa}\right)^2 & \text{at small } N/\kappa \\ -\left(\ln\frac{N}{\kappa}\right)^2\left(\frac{N}{\kappa}\right)^{-1} & \text{at large } N/\kappa \end{cases} \quad (85)$$

$${R_e}^2 - {R_e}^{2*} = \begin{cases} -\frac{37}{750}\left(\frac{N}{\kappa}\right) & \text{at small } N/\kappa \\ \frac{305-\sqrt{105}}{46}\left(\ln\frac{N}{\kappa}\right)^2\left(\frac{N}{\kappa}\right)^{-1} & \text{at large } N/\kappa \end{cases} \quad (86)$$

dx.doi.org/10.1021/ma201310e |Macromolecules 2011, 44, 7837–7852

$$R_g^2 - R_g^{2*} = \begin{cases} -\frac{4}{1125}\left(\frac{N}{\kappa}\right) & \text{at small } N/\kappa \\ \frac{75-\sqrt{105}}{69}\left(\ln\frac{N}{\kappa}\right)\left(\frac{N}{\kappa}\right)^{-1} & \text{at large } N/\kappa \end{cases} \quad (87)$$

The limiting behaviors of $h - h^*$ can be obtained from its linear relation with $\phi_1 - \phi_1^*$ and $\phi_2 - \phi_2^*$.

AUTHOR INFORMATION

Corresponding Author

*E-mail: q.wang@colostate.edu.

ACKNOWLEDGMENT

B.L. acknowledges the financial support for this work provided by the National Science Fund for Distinguished Young Scholars of China (No. 20925414), and Q.W. acknowledges the financial support provided by NSF CAREER Award CBET-0847016.

REFERENCES

(1) See, for example: Advincula, R. C., Brittain, W. J., Caster, K. C., Ruhe, J., Eds. *Polymer Brushes: Synthesis, Characterization, Applications*; Wiley-VCH: New York, 2004. Napper, D. H. *Polymeric Stabilization of Colloidal Dispersions*; Academic Press: London, 1983.

(2) See, for example: Milner, S. T. *Science* **1991**, *251*, 905. Halperin, A.; Tirrell, M.; Lodge, T. P. *Adv. Polym. Sci.* **1992**, *100*, 31. Zhao, B.; Brittain, W. J. *Prog. Polym. Sci.* **2000**, *25*, 677. Ruhe, J.; Ballauff, M.; Biesalski, M.; Dziezok, P.; Grohn, F.; Johannsmann, D.; Houbenov, N.; Hugenberg, N.; Konradi, R.; Minko, S.; Motornov, M.; Netz, R. R.; Schmidt, M.; Seidel, C.; Stamm, M.; Stephan, T.; Usov, D.; Zhang, H. N. *Adv. Polym. Sci.* **2004**, *165*, 79. Zhang, M. F.; Muller, A. H. E. *J. Polym. Sci., Part A: Polym. Chem.* **2005**, *43*, 3461.

(3) Alexander, S. *J. Phys.-Paris* **1977**, *38*, 983.

(4) de Gennes, P. G. *Macromolecules* **1980**, *13*, 1069.

(5) Carignano, M. A.; Szleifer, I. *J. Chem. Phys.* **1993**, *98*, 5006.

(6) Cherepanova, T. A.; Stekolnikov, A. V. *Mol. Phys.* **1994**, *83*, 1065.

(7) McCoy, J. D.; Ye, Y.; Curro, J. G. *J. Chem. Phys.* **2002**, *117*, 2975.

(8) Ye, Y.; McCoy, J. D.; Curro, J. G. *J. Chem. Phys.* **2003**, *119*, 555.

(9) Fredrickson, G. H. *The Equilibrium Theory of Inhomogeneous Polymers*; Oxford University Press: Oxford, U.K., 2006.

(10) Dolan, A. K.; Edwards, S. F. *P. R. Soc. London, Ser. A* **1975**, *343*, 427.

(11) Whitmore, M. D.; Noolandi, J. *Macromolecules* **1990**, *23*, 3321.

(12) Baranowski, R.; Whitmore, M. D. *J. Chem. Phys.* **1995**, *103*, 2343.

(13) Baranowski, R.; Whitmore, M. D. *J. Chem. Phys.* **1998**, *108*, 9885.

(14) Whitmore, M. D.; Baranowski, R. *Macromol. Theory Simul.* **2005**, *14*, 75.

(15) Pepin, M. P.; Whitmore, M. D. *J. Chem. Phys.* **1999**, *111*, 10381.

(16) Semenov, A. N. *Sov. Phys. JETP* **1985**, *61*, 733.

(17) Milner, S. T.; Witten, T. A.; Cates, M. E. *Europhys. Lett.* **1988**, *5*, 413.

(18) Milner, S. T.; Witten, T. A.; Cates, M. E. *Macromolecules* **1988**, *21*, 2610.

(19) Skvortsov, A. M.; Pavlushkov, I. V.; Gorbunov, A. A.; Zhulina, E. B.; Borisov, O. V.; Pryamitsyn, V. A. *Polym. Sci. USSR* **1988**, *30*, 1706.

(20) Zhulina, E. B.; Borisov, O. V.; Pryamitsyn, V. A.; Birshtein, T. M. *Macromolecules* **1991**, *24*, 140.

(21) Zhulina, E. B.; Pryamitsyn, V. A.; Borisov, O. V. *Polym. Sci. USSR* **1989**, *31*, 205.

(22) Netz, R. R.; Schick, M. *Europhys. Lett.* **1997**, *38*, 37.

(23) Netz, R. R.; Schick, M. *Macromolecules* **1998**, *31*, 5105.

(24) Likhtman, A. E.; Semenov, A. N. *Europhys. Lett.* **2000**, *51*, 307.

(25) Kim, J. U.; Matsen, M. W. *Eur. Phys. J. E* **2007**, *23*, 135.

(26) Shim, D. F. K.; Cates, M. E. *J. Phys.-Paris* **1989**, *50*, 3535.

(27) Amoskov, V. M.; Pryamitsyn, V. A. *J. Chem. Soc. Faraday Trans.* **1994**, *90*, 889.

(28) Amoskov, V. M.; Pryamitsyn, V. A. *Polym. Sci. Ser. A* **1995**, *37*, 731.

(29) Amoskov, V. M.; Pryamitsyn, V. A. *Macromol. Theory Simul.* **2003**, *12*, 223.

(30) Biesheuvel, P. M.; de Vos, W. M.; Amoskov, V. M. *Macromolecules* **2008**, *41*, 6254.

(31) Scheutjens, J. M. H. M.; Fleer, G. J. *J. Phys. Chem.* **1979**, *83*, 1619. Scheutjens, J. M. H. M.; Fleer, G. J. *J. Phys. Chem.* **1980**, *84*, 178.

(32) Cosgrove, T.; Heath, T.; Vanlent, B.; Leermakers, F.; Scheutjens, J. *Macromolecules* **1987**, *20*, 1692.

(33) Gorbunov, A. A.; Pavlushkov, I. V.; Skvortsov, A. M. *Polym. Sci. USSR* **1988**, *30*, 414.

(34) Skvortsov, A. M.; Pavlushkov, I. V.; Gorbunov, A. A. *Polym. Sci. USSR* **1988**, *30*, 487.

(35) Hirz, S. J. *Masters Thesis*, University of Minnesota, 1986.

(36) Huang, K. L.; Balazs, A. C. *Macromolecules* **1993**, *26*, 4736.

(37) Martin, J. I.; Wang, Z. G. *J. Phys. Chem.* **1995**, *99*, 2833.

(38) Milner, S. T. *J. Chem. Soc., Faraday Trans.* **1990**, *86*, 1349.

(39) Wijmans, C. M.; Scheutjens, J.; Zhulina, E. B. *Macromolecules* **1992**, *25*, 2657.

(40) Murat, M.; Grest, G. S. *Macromolecules* **1989**, *22*, 4054.

(41) Grest, G. S.; Murat, M. *Macromolecules* **1993**, *26*, 3108.

(42) Grest, G. S. *Macromolecules* **1994**, *27*, 418.

(43) Seidel, C.; Netz, R. R. *Macromolecules* **2000**, *33*, 634.

(44) Kreer, T.; Metzger, S.; Muller, M.; Binder, K.; Baschnagel, J. *J. Chem. Phys.* **2004**, *120*, 4012.

(45) He, G. L.; Merlitz, H.; Sommer, J. U.; Wu, C. X. *Macromolecules* **2007**, *40*, 6721.

(46) Dimitrov, D. I.; Milchev, A.; Binder, K. *J. Chem. Phys.* **2007**, *127*, 084905.

(47) He, G. L.; Merlitz, H.; Sommer, J. U.; Wu, C. X. *Eur. Phys. J. E* **2007**, *24*, 325.

(48) Neelov, I. M.; Binder, K. *Macromol. Theory Simul.* **2005**, *4*, 119.

(49) Pal, S.; Seidel, C. *Macromol. Theory Simul.* **2006**, *15*, 668.

(50) Chakrabarti, A.; Toral, R. *Macromolecules* **1990**, *23*, 2016.

(51) Milik, M.; Kolinski, A.; Skolnick, J. *J. Chem. Phys.* **1990**, *93*, 4440.

(52) Lai, P. Y.; Binder, K. *J. Chem. Phys.* **1991**, *95*, 9288.

(53) Lai, P. Y.; Binder, K. *J. Chem. Phys.* **1992**, *97*, 586.

(54) Pakula, T. *Macromol. Symp.* **1999**, *139*, 49.

(55) Huh, J.; Ahn, C. H.; Jo, W. H.; Bright, J. N.; Williams, D. R. *Macromolecules* **2005**, *38*, 2974.

(56) Ohno, K.; Sakamoto, T.; Minagawa, T.; Okabe, Y. *Macromolecules* **2007**, *40*, 723.

(57) Coluzza, I.; Hansen, J. P. *Phys. Rev. Lett.* **2008**, *100*, 016104.

(58) Karaiskos, E.; Bitsanis, I. A.; Anastasiadis, S. H. *J. Polym. Sci., Part B: Polym. Phys.* **2009**, *47*, 2449.

(59) Weinhold, J. D.; Kumar, S. K. *J. Chem. Phys.* **1994**, *101*, 4312.

(60) Laradji, M.; Guo, H.; Zuckermann, M. J. *Phys. Rev. E* **1994**, *49*, 3199.

(61) Soga, K. G.; Guo, H.; Zuckermann, M. J. *Europhys. Lett.* **1995**, *29*, 531.

(62) Lai, P. Y.; Zhulina, E. B. *J. Phys. II* **1992**, *2*, 547.

(63) Wang, Q.; Yin, Y. *J. Chem. Phys.* **2009**, *130*, 104903.

(64) Wang, Q. *Soft Matter* **2009**, *5*, 4564. Wang, Q. *Soft Matter* **2010**, *6*, 6206.

(65) Zhang, P.; Zhang, X.; Li, B.; Wang, Q. *Soft Matter* **2011**, *7*, 4461.

(66) Zhang, P.; Li, B.; Wang, Q. *Macromolecules*, to be submitted.

(67) Helfand, E.; Tagami, Y. *J. Polym. Sci., Part B: Polym. Lett.* **1971**, *9*, 741. Helfand, E.; Tagami, Y. *J. Chem. Phys.* **1972**, *56*, 3592.

(68) Frenkel, D.; Smit, B. *Understanding Molecular Simulation -- From Theory to Applications*; Academic Press: New York, 2002.

(69) Shell, M. S.; Debenedetti, P. G.; Panagiotopoulos, A. Z. *J. Chem. Phys.* **2003**, *119*, 9406.
(70) Ghulghazaryan, R. G.; Hayryan, S.; Hu, C. *J. Comput. Chem.* **2007**, *28*, 715.
(71) Chipot, C.; Pohorille, A., Eds. *Free Energy Calculations: Theory and Applications in Chemistry and Biology*; Springer: Berlin, 2007; Chapter 3.
(72) Jain, T. S.; de Pablo, J. J. *J. Chem. Phys.* **2002**, *116*, 7238.
(73) Press, W. H.; Teukolsky, S. A.; Vetterling, W. T.; Flannery, B. P. *Numerical Recipes in FORTRAN: the Art of Scientific Computing*; Cambridge University Press: Cambridge, U.K., 2002.